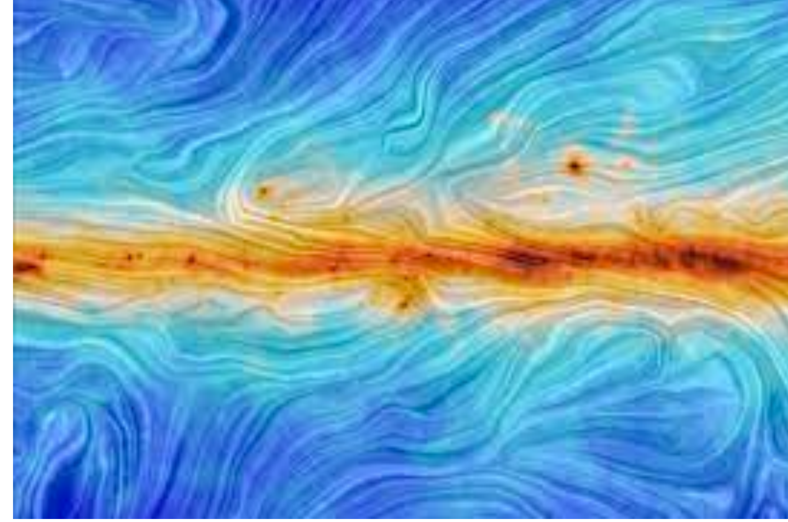

Chiral Magnetic Fields in the Early Universe: Evolution and Signatures

Tina Kahniashvili
Carnegie Mellon University (USA)
&
Ilia State University (Georgia)

Stony Brook
Nov. 3 2021

outline

- why primordial (chiral) magnetic fields?
  - observations vs theory
- early universe magnetogenesis
  - inflation
  - phase transitions
  - Chiral magnetic effect
- primordial turbulence
  - vorticities
  - magnetic fields
- evolution
  - decay
  - amplification
- signatures
  - cosmic microwave background
  - gravitational waves
  - cosmic magnetic fields

Senior Collaborators

- Nick Battaglia
- Alexey Boayrsky
- Axel Brandenburg
- Marcus Brüggen
- Leonardo Campanelli
- Ruth Durrer
- Jurg Frohlich
- Grigol Gogoberidze
- Nathanie Kleorin
- Arthur Kosowsky
- Andrii Neronov
- Bharat Ratra
- Igor Rogachevskii
- Oleg Ruchayskirsky
- Shane O'Sullivan
- Wolfram Schmidt
- Jennifer Schober
- Alexander Tevzadze
- Tanmay Vachaspati

Junior Collaborators

- Emma Clarke
- Paola Dominigues-Fernandez
- Yutong He
- Xialong Du
- Sayan Mandal
- Salome Mtchedlidze
- Alberto Roper Pol
- Nakul Shenoy
- Jonathan Stepp
- Winston Yin

NSF
NASA
Vetenskapsrådet
Swedish Research Council
SRNSFG
CARNEGIE MELLON UNIVERSITY
PITTSBURGH PENNSYLVANIA 1900
1737
NORDITA
The Nordic Institute for Theoretical Physics
PUBLICA HELIAE UNIVERSITAS
LIGAMUS

Observational Overview

cosmic magnetism

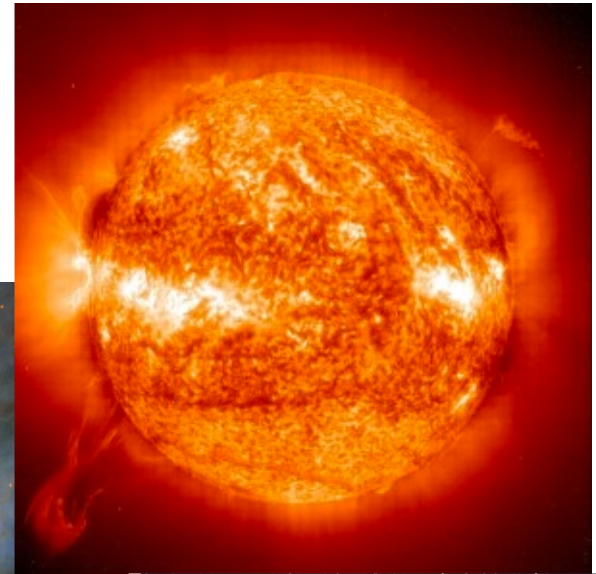

why primordial magnetic fields?

- cosmic *seed* magnetic fields
  - astrophysical seeds
  - cosmological seeds
- observations
  - Fermi data – blazars spectra

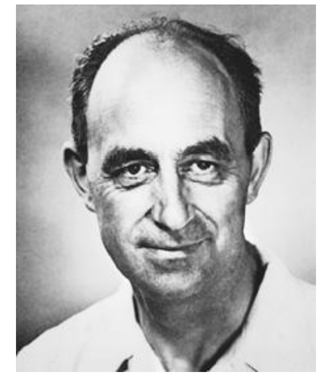

PHYSICAL REVIEW VOLUME 75, NUMBER 8 APRIL 15, 1949

On the Origin of the Cosmic Radiation

ENRICO FERMI
Institute for Nuclear Studies, University of Chicago, Chicago, Illinois

(Received January 3, 1949)

A theory of the origin of cosmic radiation is proposed according to which cosmic rays are originated and accelerated primarily in the interstellar space of the galaxy by collisions against moving magnetic fields. One of the features of the theory is that it yields naturally an inverse power law for the spectral distribution of the cosmic rays. The chief difficulty is that it fails to explain in a straightforward way the heavy nuclei observed in the primary radiation.

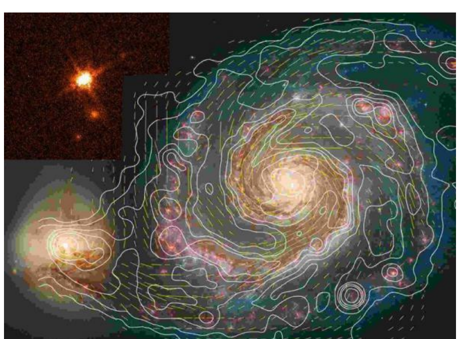

E. Fermi
***"On the origin of the cosmic radiation"*,**
PRD, 75, 1169 (1949)

observations: Fermi data

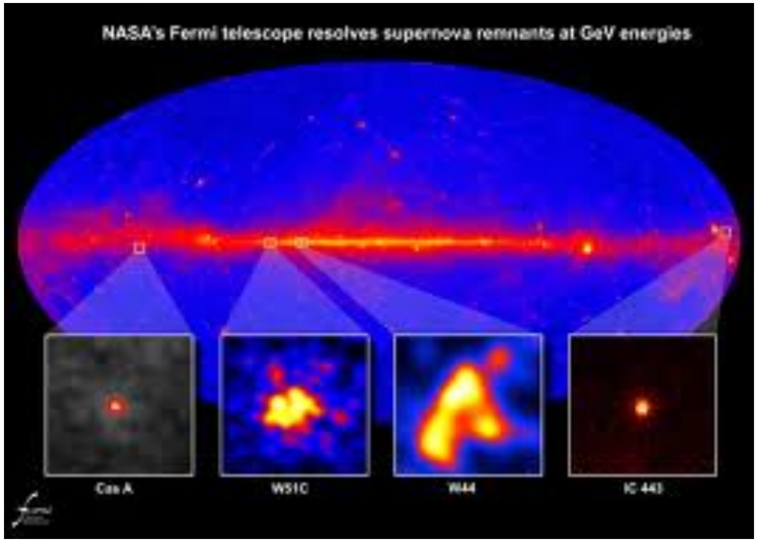

$$\gamma + \gamma \rightarrow e^{+} + e^{-}$$

Neronov and Vovk 2010

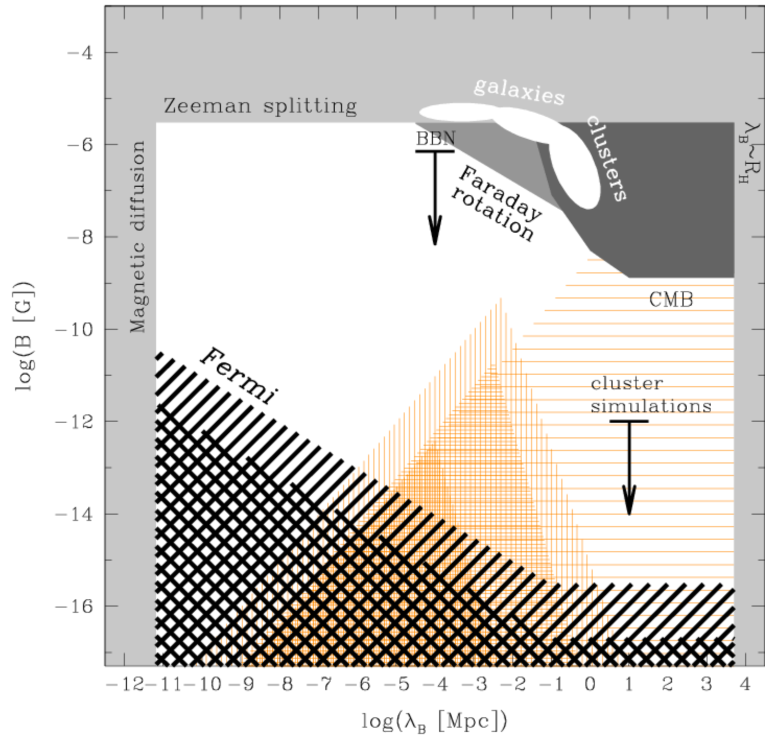

A&A 529, A144 (2011)
DOI: 10.1051/0004-6361/201116441

Astronomy & Astrophysics

Extragalactic magnetic fields constraints from simultaneous GeV–TeV observations of blazars

A. M. Taylor[1], I. Vovk[1], and A. Neronov[1]

ISDC Data Centre for Astrophysics, Ch. d'Ecogia 16, 1290 Versoix, Switzerland
e-mail: Andrew.Taylor@unige.ch

Received 5 January 2011 / Accepted 18 March 2011

ABSTRACT

Context. Attenuation of the TeV γ-ray flux from distant blazars through pair production with extragalactic background light leads to the development of electromagnetic cascades and subsequent, lower energy, GeV secondary γ-ray emission. Due to the deflection of VHE cascade electrons by extragalactic magnetic fields (EGMF), the spectral shape of this arriving cascade γ-ray emission is dependent on the strength of the EGMF. Thus, the spectral shape of the GeV–TeV emission from blazars has the potential to probe the EGMF strength along the line of sight to the object. Constraints on the EGMF previously derived from the gamma-ray data suffer from an uncertainty related to the non-simultaneity of GeV and TeV band observations.
Aims. We investigate constraints on the EGMF derived from observations of blazars for which TeV observations simultaneous with those by *Fermi* telescope were reported. We study the dependence of the EGMF bound on the hidden assumptions it rests upon.
Methods. We select blazar objects for which simultaneous Fermi/LAT GeV and Veritas, MAGIC or HESS TeV emission have been published. We model the development of electromagnetic cascades along the gamma-ray beams from these sources using Monte Carlo simulations, including the calculation of the temporal delay incurred by cascade photons, relative to the light propagation time of direct γ-rays from the source.
Results. Constraints on the EGMF could be derived from the simultaneous GeV–TeV data on the blazars RGB J0710+591, 1ES 0229+200, and 1ES 1218+304. The measured source flux level in the GeV band is lower than the flux of the expected cascade component calculated under the assumption of zero EGMF. Assuming that the reason for the suppression of the cascade component is the extended nature of the cascade emission, we find that $B \gtrsim 10^{-15}$ G (assuming an EGMF correlation length of $\geq$1 Mpc) is consistent with the data. Alternatively, the assumption that the suppression of the cascade emission is caused by the time delay of the cascade photons the data are consistent with $B \gtrsim 10^{-17}$ G for the same correlation length.

Key words. astroparticle physics – magnetic fields – radiative transfer

The Astrophysical Journal Letters, 733:L21 (5pp), 2011 June 1 doi:10.1088/2041-8205/733/2/L21

TIME DELAY OF CASCADE RADIATION FOR TeV BLAZARS AND THE MEASUREMENT OF THE INTERGALACTIC MAGNETIC FIELD

Charles D. Dermer[1], Massimo Cavadini[2], Soebur Razzaque[1,6], Justin D. Finke[1], James Chiang[3], and Benoit Lott[4,5]
[1] Space Science Division, U.S. Naval Research Laboratory, Washington, DC 20375, USA; charles.dermer@nrl.navy.mil
[2] Dipartimento di Fisica e Matematica, Universitá dell'Insubria, via Valleggio 11, 22100, Como, Italy
[3] W. W. Hansen Experimental Physics Laboratory, Kavli Institute for Particle Astrophysics and Cosmology, Department of Physics and SLAC National Accelerator Laboratory, Stanford University, Stanford, CA 94305, USA
[4] CNRS/IN2P3, Centre d' Études Nucléaires Bordeaux Gradignan, UMR 5797, Gradignan, 33175, France
[5] 40 Université de Bordeaux, Centre d' Études Nucléaires Bordeaux Gradignan, UMR 5797, Gradignan, 33175, France
Received 2010 November 27; accepted 2011 April 7; published 2011 May 6

ABSTRACT

Recent claims that the strength $B_{\rm IGMF}$ of the intergalactic magnetic field (IGMF) is $\gtrsim 10^{-15}$ G are based on upper limits to the expected cascade flux in the GeV band produced by blazar TeV photons absorbed by the extragalactic background light. This limit depends on an assumption that the mean blazar TeV flux remains constant on timescales $\gtrsim 2(B_{\rm IGMF}/10^{-18}{\rm G})^2/(E/10\ {\rm GeV})^2$ yr for an IGMF coherence length $\approx$1 Mpc, where E is the measured photon energy. Restricting TeV activity of 1ES 0229+200 to $\approx$3–4 years during which the source has been observed leads to a more robust lower limit of $B_{\rm IGMF} \gtrsim 10^{-18}$ G, which can be larger by an order of magnitude if the intrinsic source flux above $\approx$5–10 TeV from 1ES 0229+200 is strong.

primordial or astrophysical origin?

E Astrophysical Journal Letters, 727:L4 (4pp), 2011 January 20 doi:10.1088/2041-8205/727/1/L4

LOWER LIMIT ON THE STRENGTH AND FILLING FACTOR OF EXTRAGALACTIC MAGNETIC FIELDS

K. Dolag[1,2], M. Kachelriess[3], S. Ostapchenko[3,4], and R. Tomàs[5]
[1] Universitätssternwarte München, München, Germany
[2] Max-Planck-Institut für Astrophysik, Garching, Germany
[3] Institutt for fysikk, NTNU, Trondheim, Norway
[4] D. V. Skobeltsyn Institute of Nuclear Physics, Moscow State University, Moscow, Russia
[5] II. Institut für Theoretische Physik, Universität Hamburg, Germany
Received 2010 September 16; accepted 2010 November 25; published 2010 December 21

ABSTRACT

High-energy photons from blazars can initiate electromagnetic pair cascades interacting with the extragalactic photon background. The charged component of such cascades is deflected and delayed by extragalactic magnetic fields (EGMFs), thereby reducing the observed point-like flux and potentially leading to multi-degree images in the GeV energy range. We calculate the fluence of 1ES 0229+200 as seen by *Fermi*-LAT for different EGMF profiles using a Monte Carlo simulation for the cascade development. The non-observation of 1ES 0229+200 by *Fermi*-LAT suggests that the EGMF fills at least 60% of space with fields stronger than $\mathcal{O}(10^{-16}$ to $10^{-15})$ G for lifetimes of TeV activity of $\mathcal{O}(10^2$ to $10^4)$ yr. Thus, the (non-)observation of GeV extensions around TeV blazars probes the EGMF in voids and puts strong constraints on the origin of EGMFs: either EGMFs were generated in a space filling manner (e.g., primordially) or EGMFs produced locally (e.g., by galaxies) have to be efficiently transported to fill a significant volume fraction as, e.g., by galactic outflows.

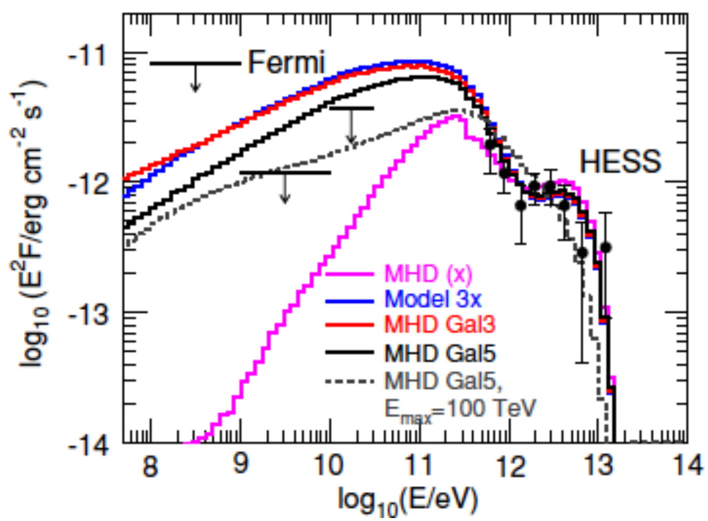

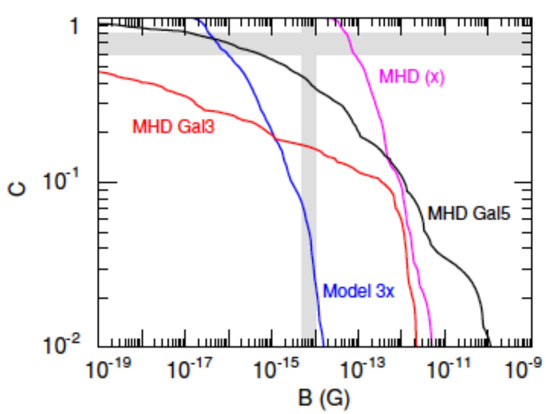

Figure 4. Cumulative volume filling factor $C(B)$ for the four different EGMF models found in MHD simulations.

(A color version of this figure is available in the online journal.)

4. SUMMARY

We have calculated the fluence of 1ES 0229+200 as seen by *Fermi*-LAT using a Monte Carlo simulation for the cascade development. We have discussed the effect of different EGMF profiles on the resulting suppression of the point-like flux seen by *Fermi*-LAT. Since the electron cooling length is much smaller than the mean free path of the TeV photons, a sufficient suppression of the point-like flux requires that the EGMF fills a large fraction along the line of sight toward 1ES 0229+200, $f \gtrsim 0.6$. The lower limit on the magnetic field strength in this volume is $B \sim \mathcal{O}(10^{-15})$ G, assuming 1ES 0229+200 is stable at least for 10^4 yr, weakening by a factor of 10 for $\tau = 10^2$ yr. These limits put very stringent constraints on the origin of EGMFs. Either the seeds for EGMFs have to be produced by a volume filling process (e.g., primordial) or very efficient transport processes have to be present which redistribute magnetic fields that were generated locally (e.g., in galaxies) into filaments and voids with a significant volume filling factor.

improved data

S. Archambault et al. [VERITAS Collaboration],
"Search for Magnetically Broadened Cascade Emission From Blazars with VERITAS," Astrophys. J. 835 , 288 (2017).

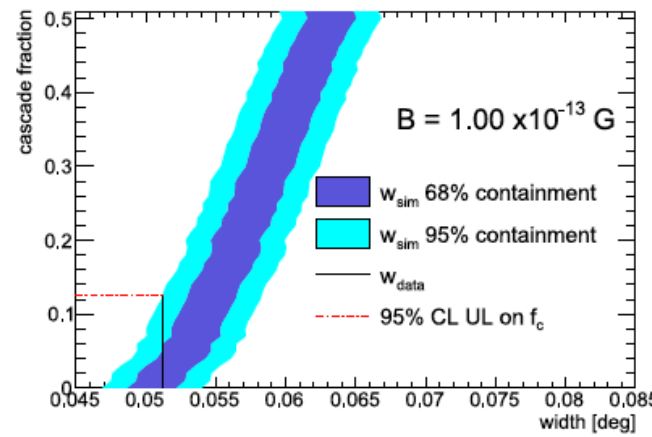

Figure 3. The dependence of the width of the simulated angular distribution on the cascade fraction f_c for 1ES 1218+304. This is compared against the width of the angular distribution measured in data, w_{data}.

M. Ackermann, et al. [Fermi-LAT Collaboration],
"The Search for Spatial Extension in High-latitude Sources Detected by the Fermi Large Area Telescope,"
Astrophys. J. Suppl. 237 , 32 (2018).

For the cutoff energy of 10 TeV assumed for the intrinsic spectrum of 1ES 1218+ 308, the first pair production interaction occurs larger 10 Mpc from the source. Consequently, this study probes the magnetic field strength in areas distant from the source, sampling cosmic voids, rather than matter-rich regions.

known vs. unknown

What we know

- The amplitude of the magnetic field
- The spectral shape of the magnetic field
- The correlation length scale

What we do not know

- When and how magnetic fields were generated
- What were initial conditions

Two Options:
Cosmological and Astrophysical Scenarios

MHD cosmological simulations

by *Donnert et al. 2008*

Ejection

Z=4

Z=0

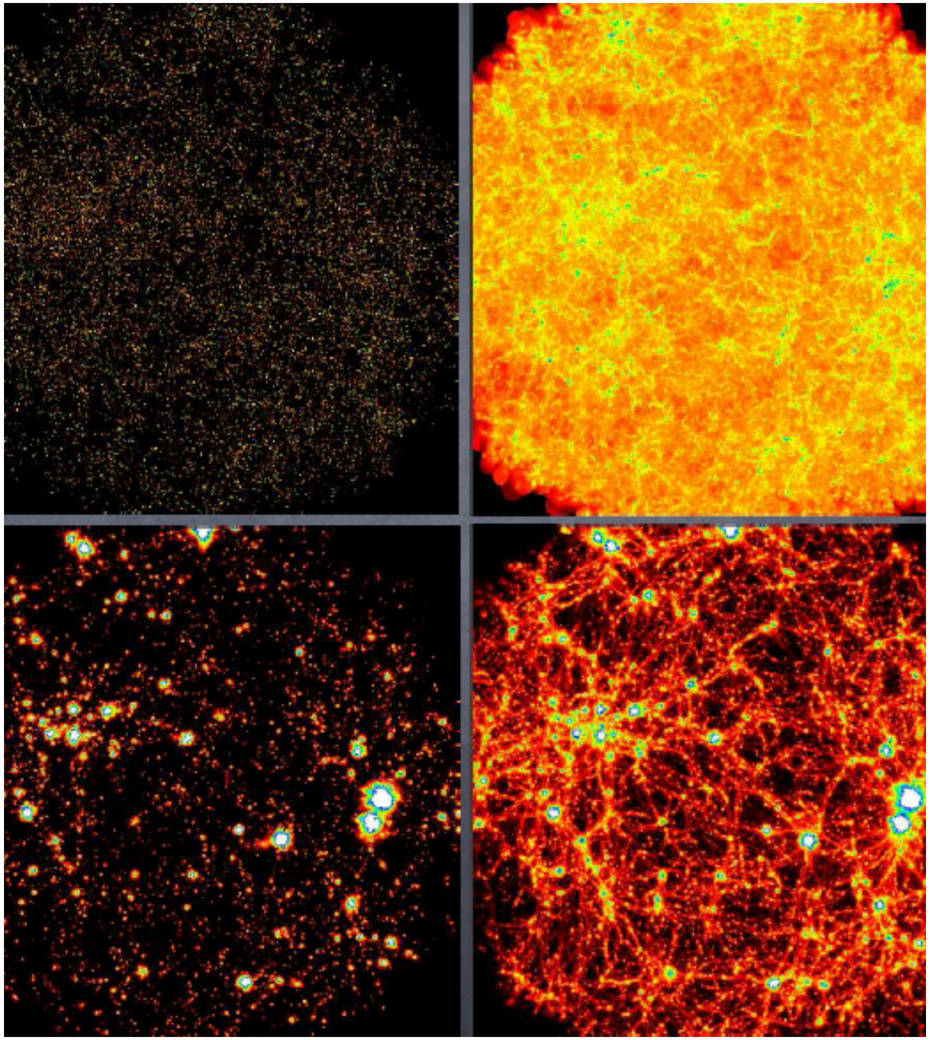

Primordial

Z=4

Z=0

Cosmological Magnetogenesis

primordial magnetogenesis

F. Hoyle in Proc. ***"La structure et l'evolution de l'Universe"*** **(1958)**

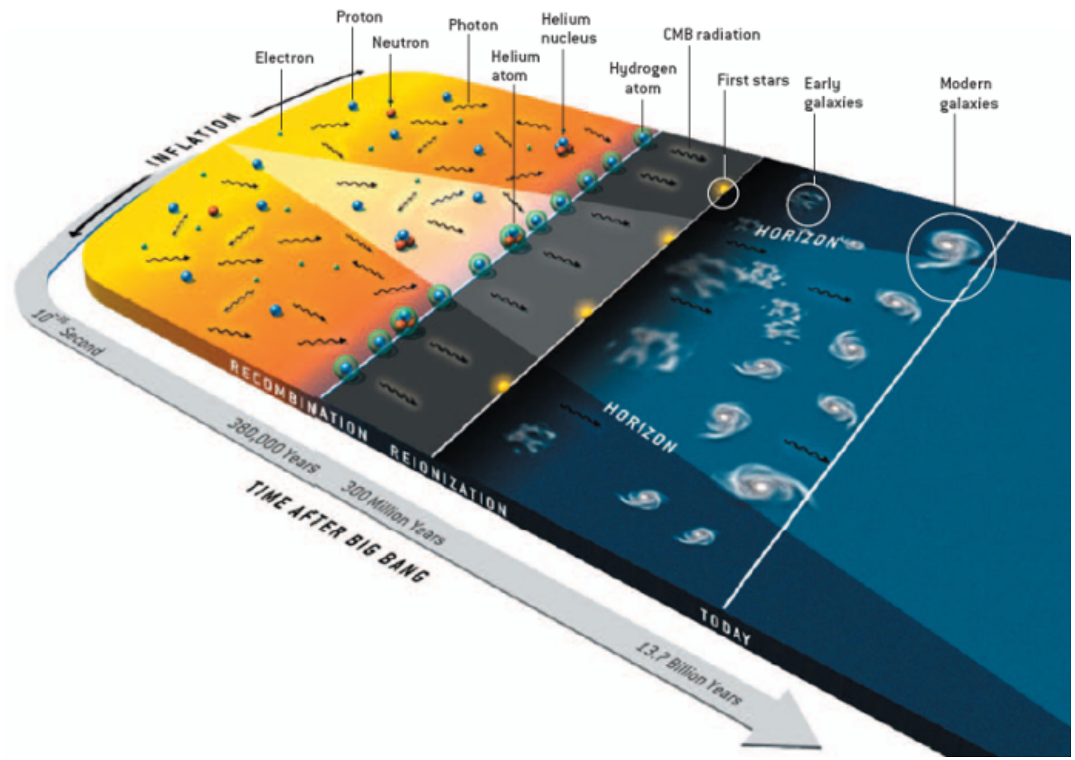

- inflation
- phase transitions
- supersymmetry
- string cosmology
- topological defects

primordial magnetogenesis

- Inflation
  - the correlation length larger than horizon
  - scale invariant spectrum
  - well agree with the lower bounds
  - difficulties:
    - backreaction & symmetries violations

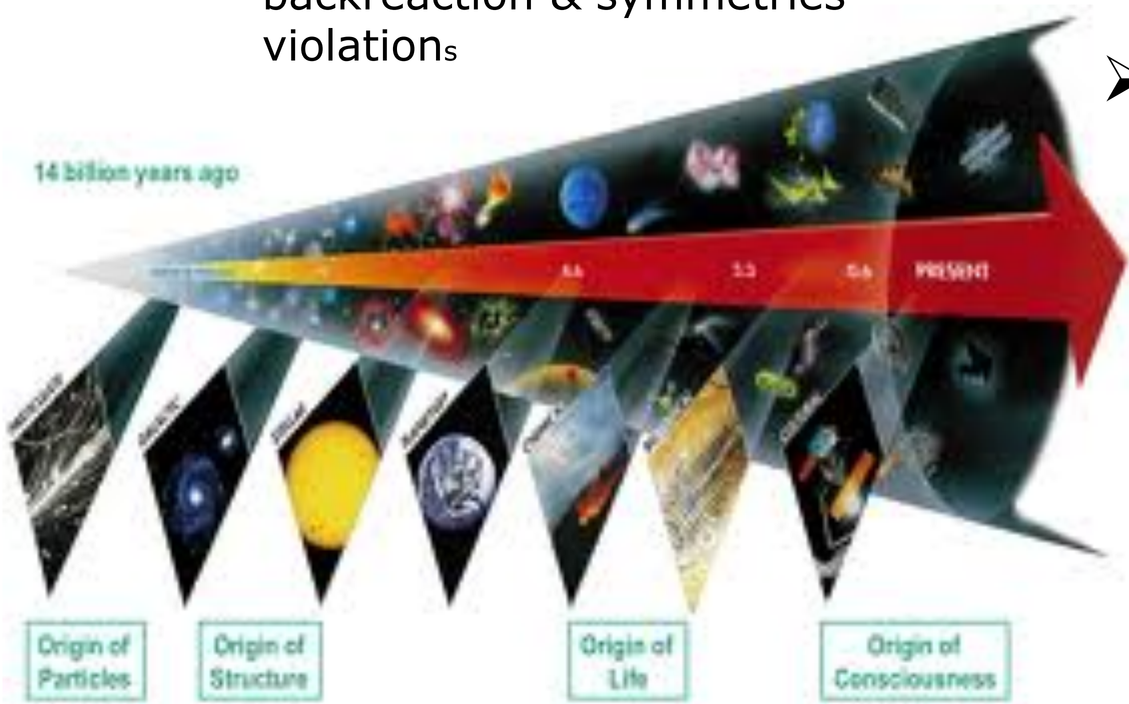

- Phase transitions
  - bubble collisions – first order phase transitions QCDPT or EWPT
  - causal fields
  - limited correlation length

- chiral magnetic effect

testing the early universe

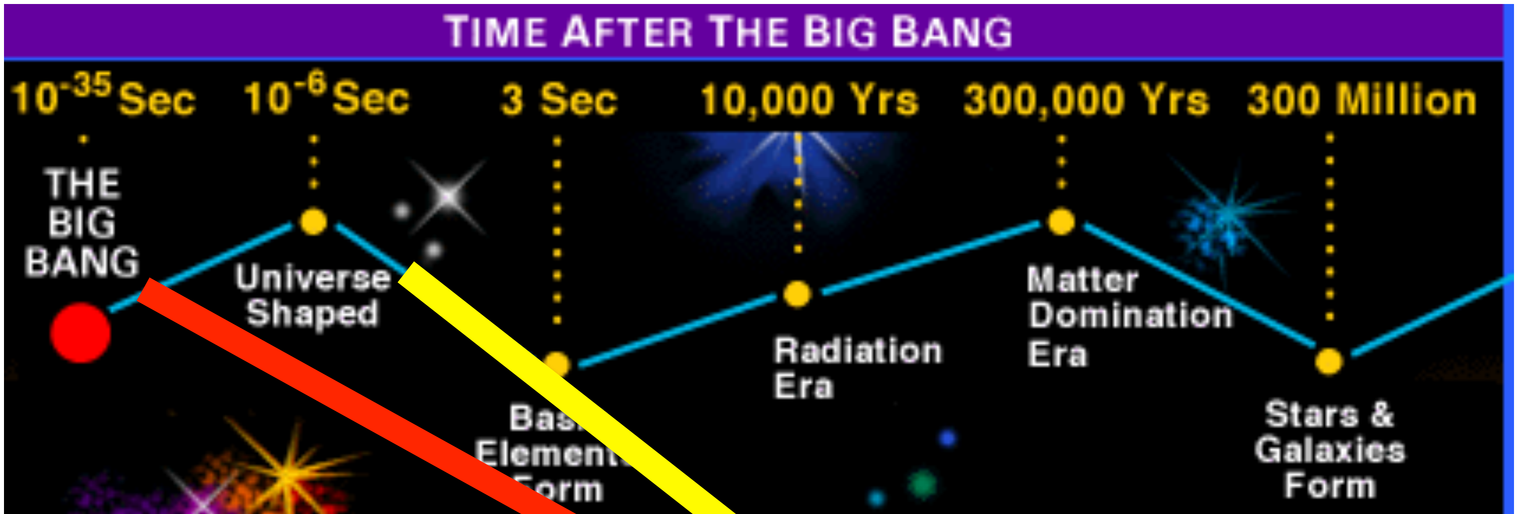

magnetic field origin
red-inflation
yellow- phase transitions

primordial MHD turbulence

- primordial plasma is perfect conductor
- interaction between primordial magnetic fields and fluid (plasma)
- development of turbulence

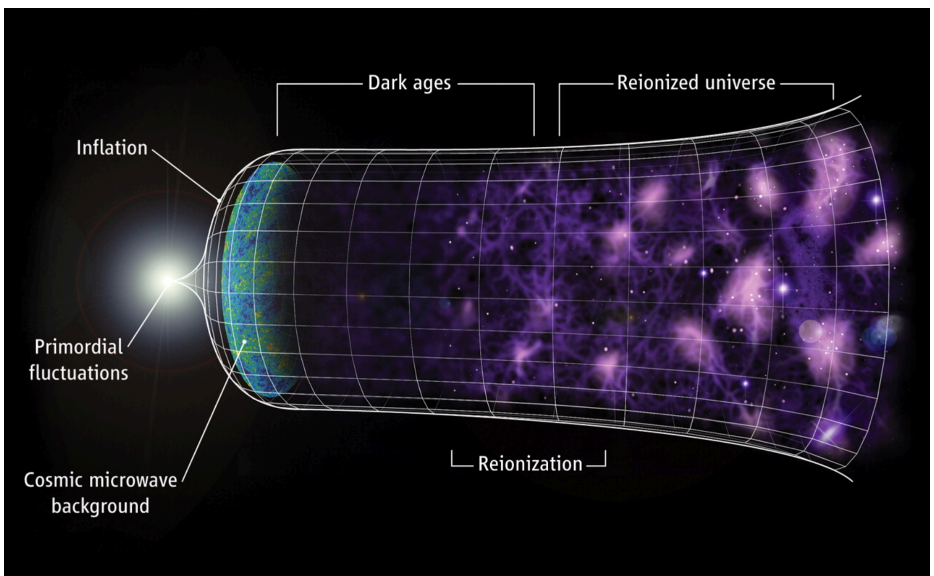

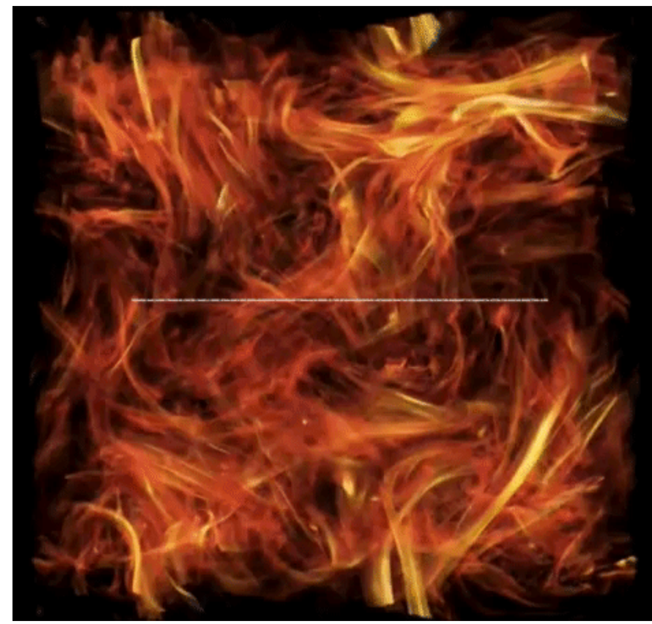

Penders, Jones, Porter, 2019

other sources of primordial turbulence?

primordial velocity field

- Cosmological Phase Transitions

Bubbles collisions and nucleation

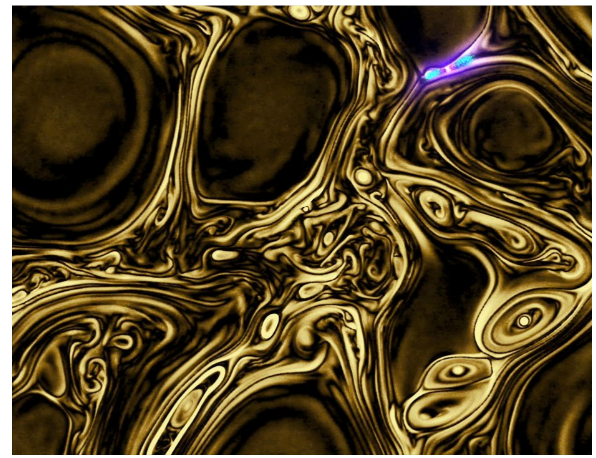

Baym et al. 1995

Quashnock, et al. 1989

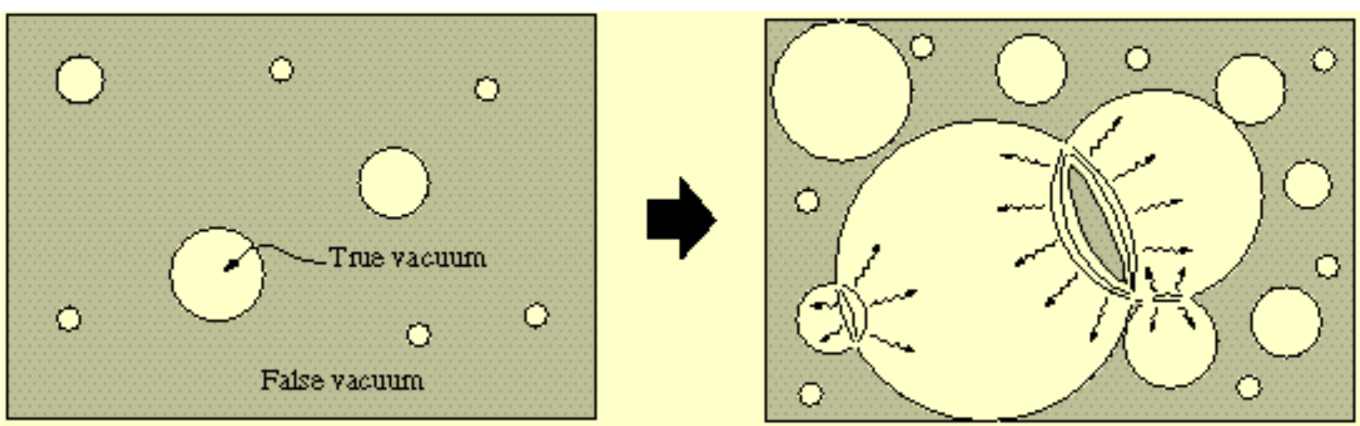

chiral magnetic effect

- ✓ Asymmetry between right- and left-handed fermions – amplification (exponential growth) of helical magnetic fields, chital magnetic effect (CME), Vilenkin 1980

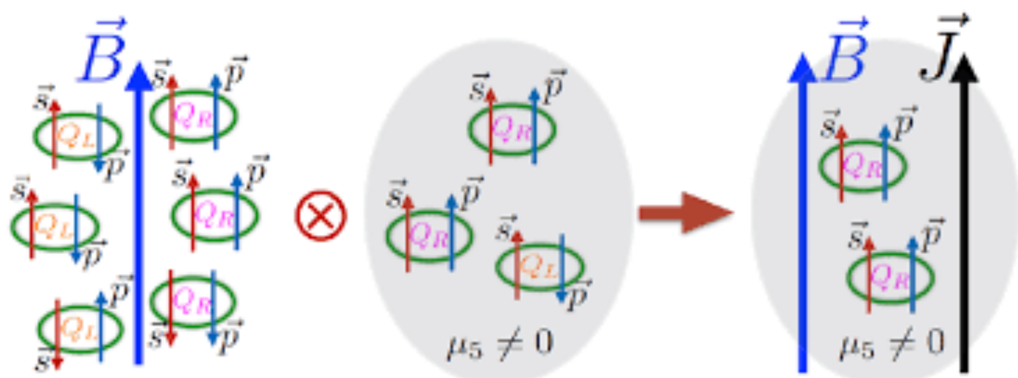

Kharzeev, Liao, Voloshin, Wang, 2015

- ✓ Magnetogenesis in the early universe – seed helical magnetic fields, *Boyarsky et al. 2012*
- ✓ Turbulent chiral magnetic inverse cascade in the early universe – *Brandenburg et al. 2017*

Primordial MHD Evolution

describing primordial turbulence

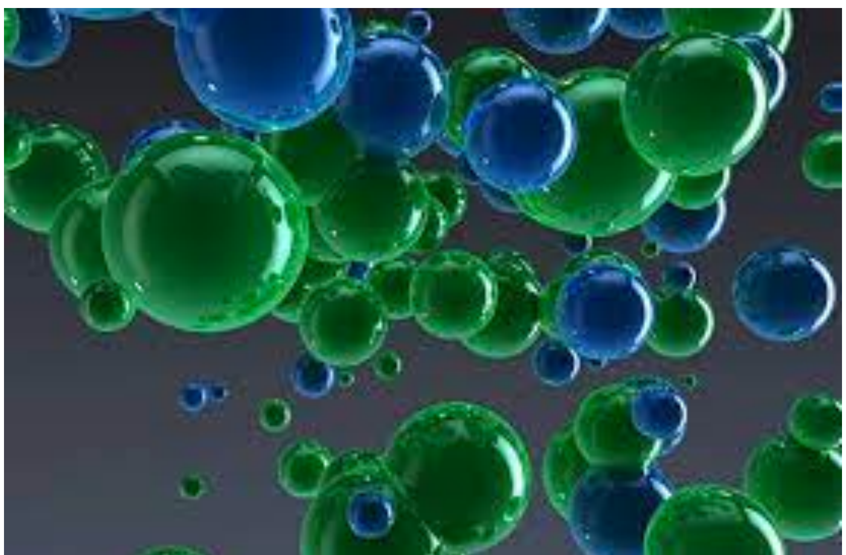

$$\frac{\partial \rho}{\partial t} + \nabla \cdot [\rho \mathbf{v}] = 0$$

$$\frac{\partial (\rho \mathbf{v})}{\partial t} + \nabla \cdot [\rho \mathbf{v}\mathbf{v} - \mathbf{B}\mathbf{B} + \mathsf{P}^*] = 0$$

$$\frac{\partial E}{\partial t} + \nabla \cdot [(E + P^*)\mathbf{v} - \mathbf{B}\,(\mathbf{B} \cdot \mathbf{v})] = 0$$

$$\frac{\partial \mathbf{B}}{\partial t} - \nabla \times (\mathbf{v} \times \mathbf{B}) = 0$$

$$P^* = P + \frac{\mathbf{B} \cdot \mathbf{B}}{2}$$

$$E = P/(\gamma - 1) + \frac{\rho(\mathbf{v} \cdot \mathbf{v})}{2} + \frac{\mathbf{B} \cdot \mathbf{B}}{2}$$

turbulence development

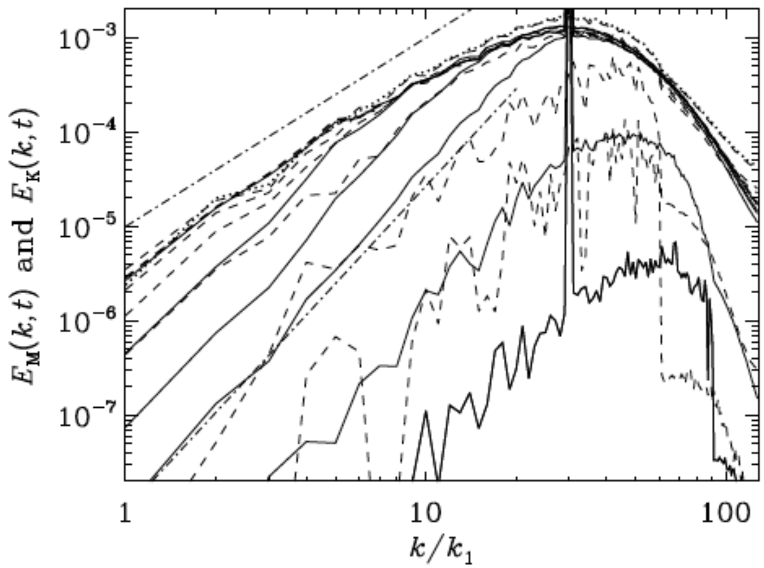

$$\frac{D\rho}{Dt} = -\rho \boldsymbol{\nabla} \cdot \mathbf{u},$$
$$\rho \frac{D\mathbf{u}}{Dt} = (\boldsymbol{\nabla} \times \mathbf{b}) \times \mathbf{b} - c_s^2 \boldsymbol{\nabla} \rho + \boldsymbol{\nabla} \cdot (2\rho\nu \mathsf{S}),$$
$$\frac{\partial \mathbf{A}}{\partial t} = \mathbf{u} \times \mathbf{b} + \eta \nabla^2 \mathbf{A},$$

where $D/Dt = \partial/\partial t + \mathbf{u} \cdot \boldsymbol{\nabla}$ is the advective derivative, t is the conformal time, ρ is the density, $\mathbf{u}$ is the bulk velocity, $\mathsf{S}_{ij} = \frac{1}{2}(u_{i,j} + u_{j,i}) - \frac{1}{3}\delta_{ij} \boldsymbol{\nabla} \cdot \mathbf{u}$ is the rate-of-strain tensor, ν is the viscosity, and η is the magnetic diffusivity.

Kahniashvili et al. 2010

7

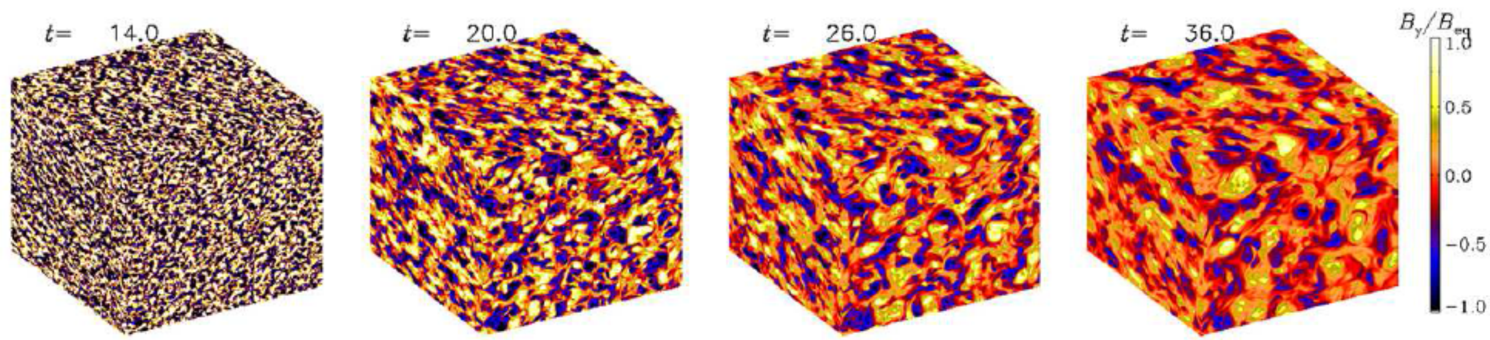

FIG. 2: Evolution of the turbulent magnetic field after turning off the forcing at time $t = 14\,t_1$. The B_y component is shown on the periphery of the computational domain.

our universe is almost perfect conductor

magnetically dominant

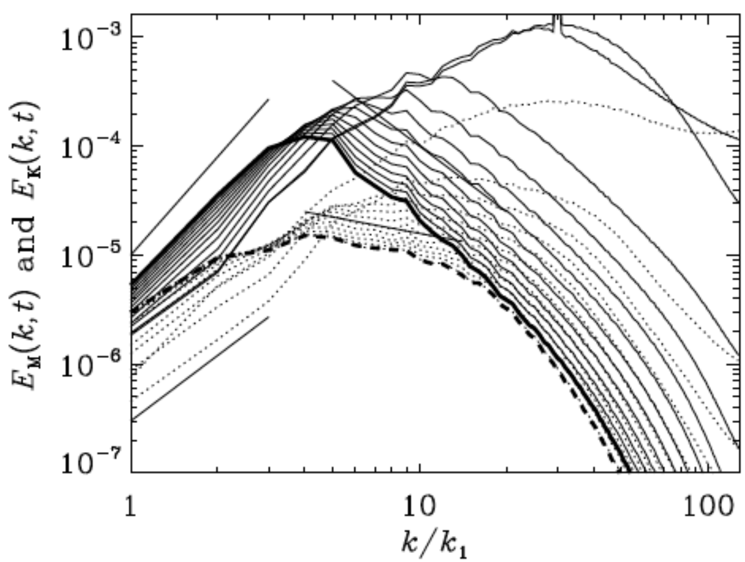

FIG. 5: Magnetic (solid) and kinetic (dashed) energy spectra in 12 regular time intervals of $4\,t_1$ after having turned off the forcing, with (smoothed) spectra at $k = 50k_1$ decreasing as t increases. $\nu = \eta = 10^{-4}$ in units of $(k_1^2 t_1)^{-1}$. The straight lines have slopes 3, 2, -2, and $-1/2$, with the first two near $k = k_1$ and the last two near $k = 10k_1$. Thickest lines (solid and dashed) indicate the last time, which is $44\,t_1$ since turning off the forcing. The intermediate thickness solid line, the highest or almost highest line for $k/k_1 > 10$, is the initial magnetic spectrum for this computation.

kinetically dominant

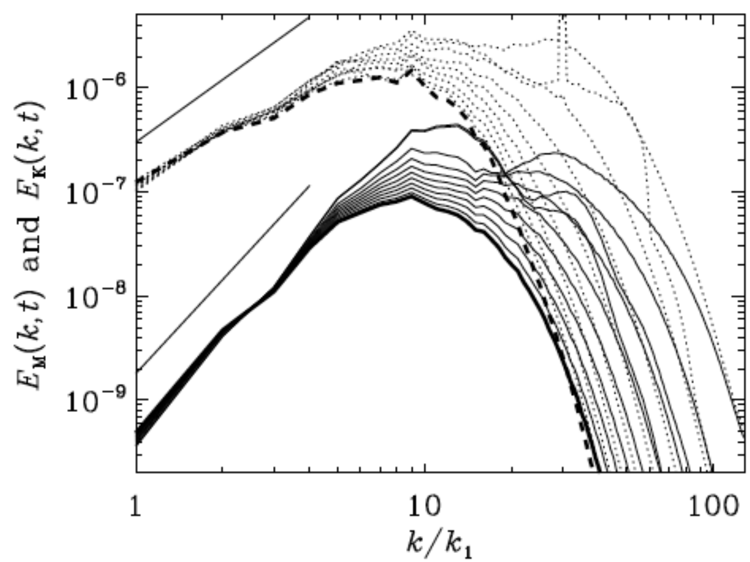

FIG. 6: Same as Fig. 5, but for a case where the initial magnetic field had a k^4 spectrum close to equipartition with the velocity field, and then the forcing was turned off. Results are shown for nine times at intervals of $6\,t_1$. $\nu = \eta = 10^{-4}$ in units of $(k_1^2 t_1)^{-1}$. The straight lines have slopes 2 and 3. Thickest lines (solid and dashed) indicate the last time, which is $48\,t_1$ since turning off the forcing. The intermediate thickness solid line, the highest solid line for $5 < k/k_1 < 10$, is the initial magnetic spectrum for this computation.

Kahniashvili et al. 2010

high resolution 3D compressible MHD simulations - decay

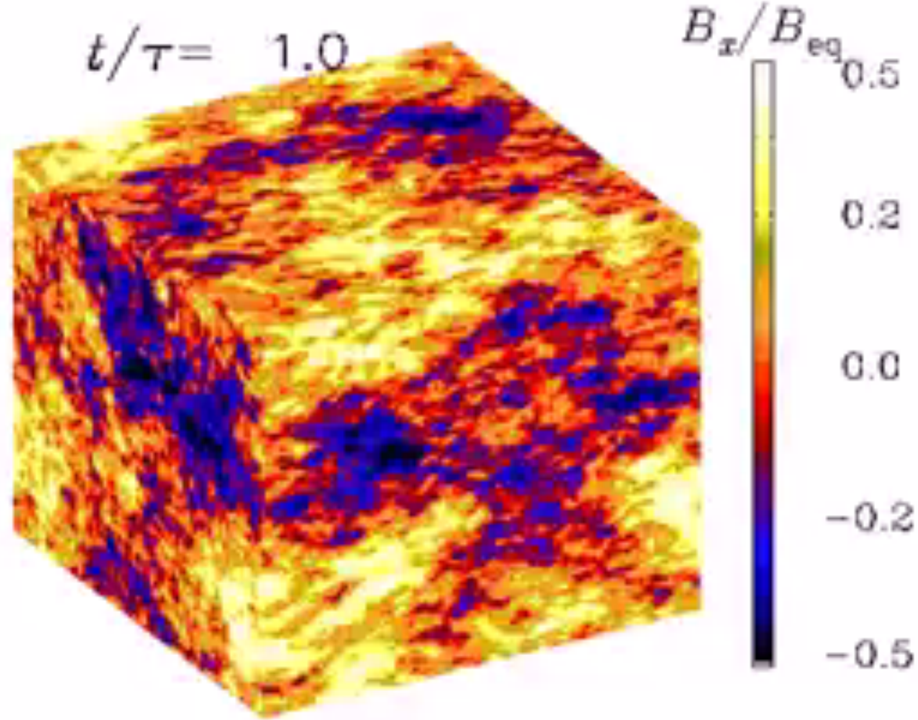

Brandenburg et al. 2015

inverse transfer

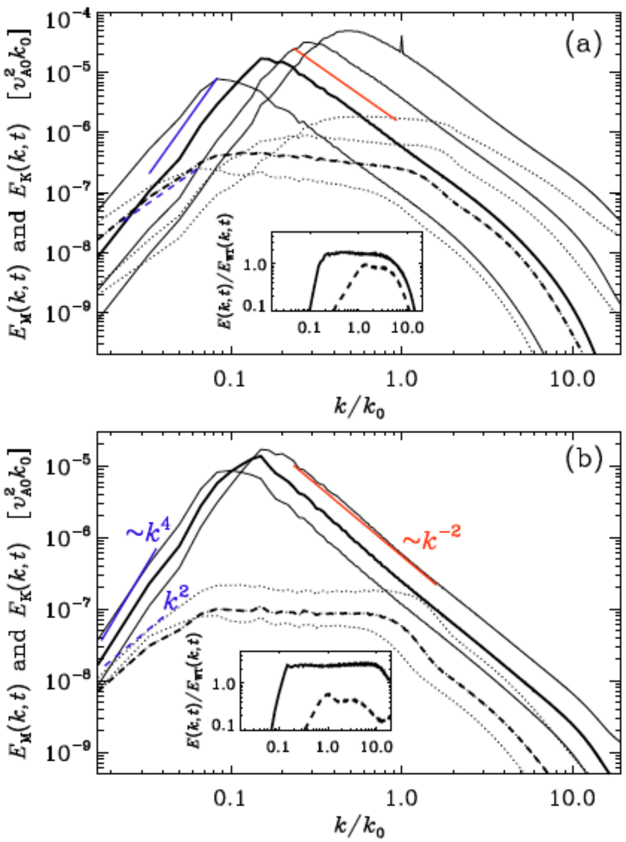

FIG. 1: (Color online) (a) Magnetic (solid lines) and kinetic (dashed lines) energy spectra for Run A at times $t/\tau_A = 18$, 130, 450, and 1800; the time $t/\tau_A = 450$ is shown as bold lines. The straight lines indicate the slopes k^4 (solid, blue), k^2 (dashed, blue), and k^{-2} (red, solid). (b) Same for Run B, at $t/\tau_A = 540$, 1300, and 1800, with $t/\tau_A = 1300$ shown as bold lines. The insets show E_M and E_K compensated by E_{WT}.

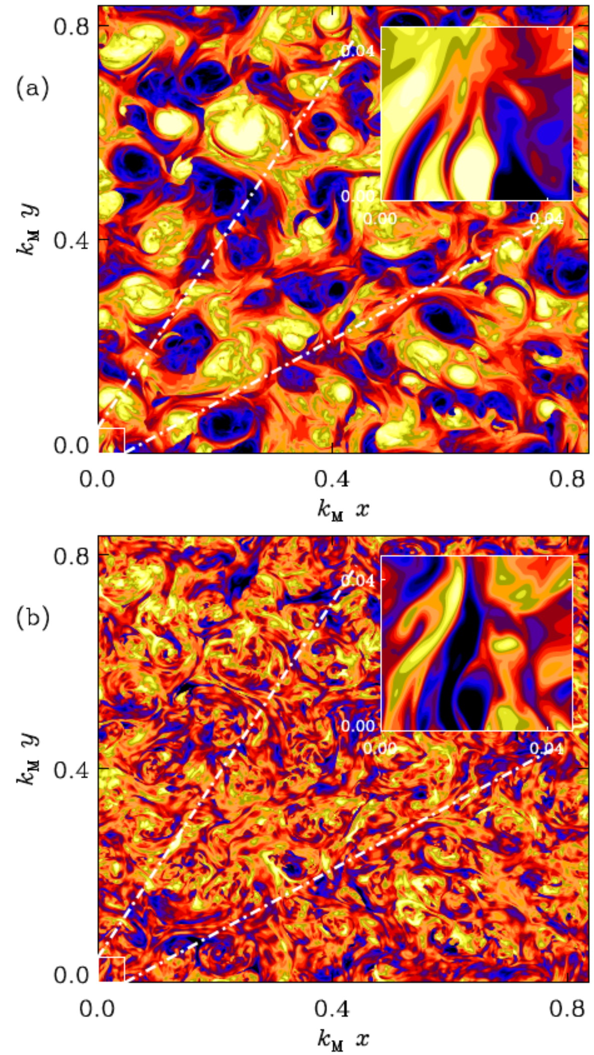

FIG. 2: (Color online) Contours of (a) $B_z(x,y)$ and (b) $u_z(x,y)$ for Run A. The insets show a zoom into the small square in the lower left corner.

Brandenburg, Kahniashvili, Tevzadze 2015

classes of turbulences

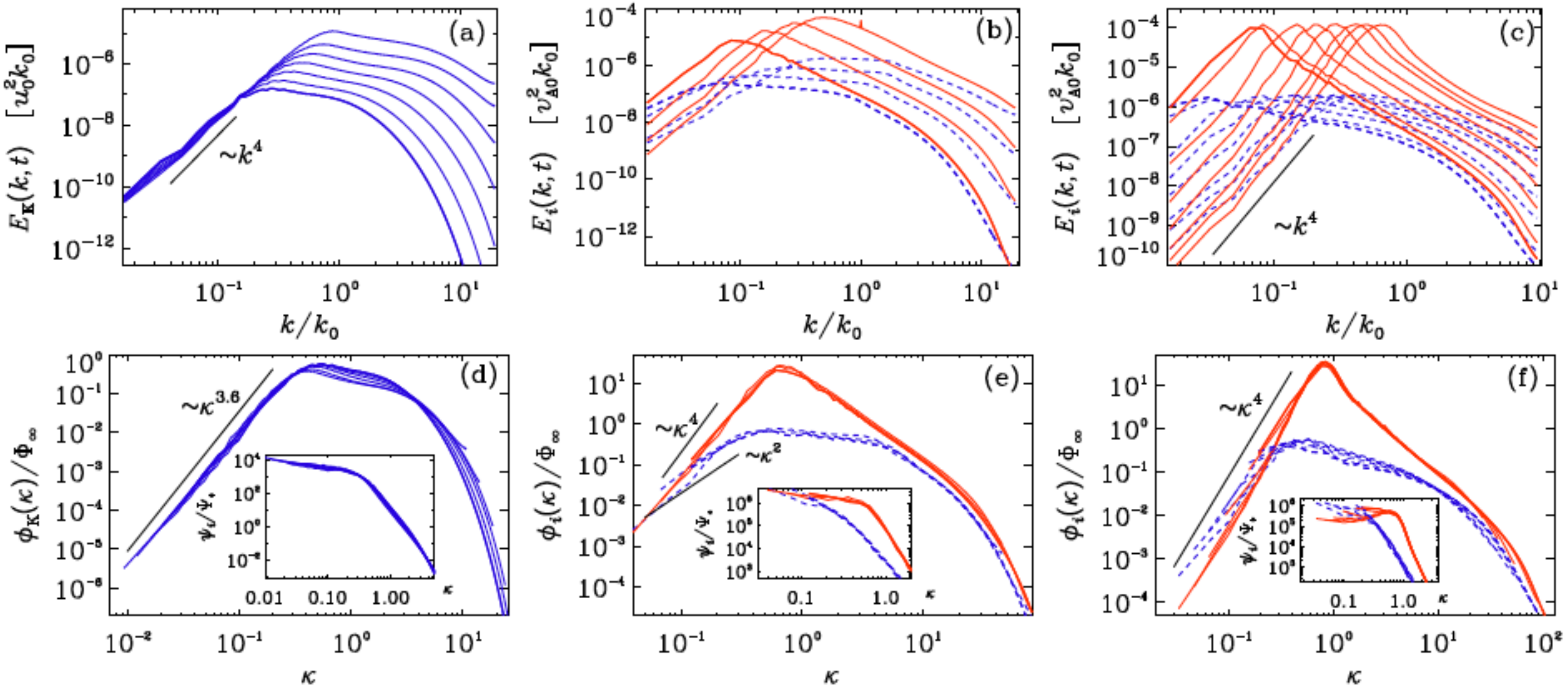

Brandenburg & Kahniashvili 2017

classes of MHD turbulence

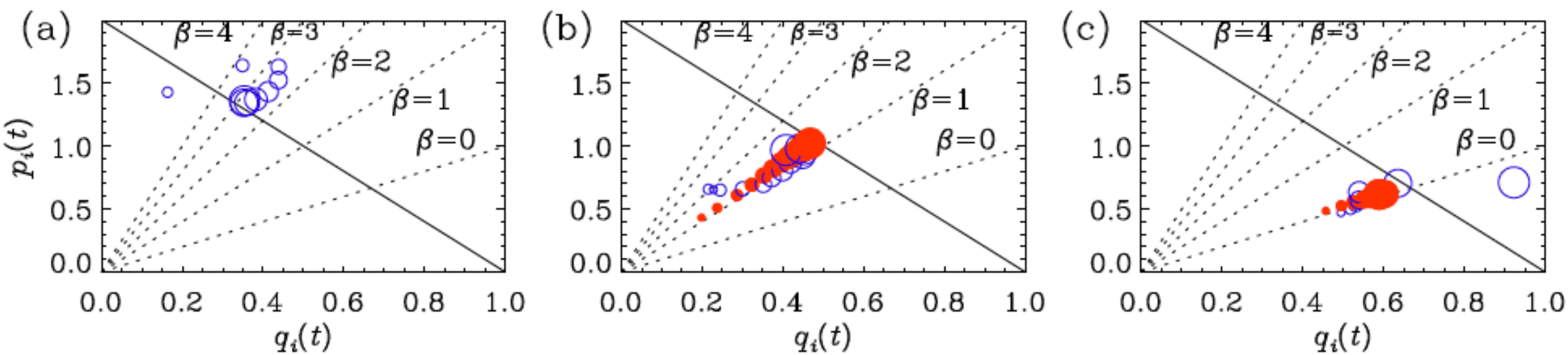

FIG. 2: pq diagrams for cases (i)–(iii). Open (closed) symbols correspond to $i = \mathrm{K}$ (M) and their sizes increase with time.

TABLE I: Scaling exponents and relation to physical invariants and their dimensions.

β	p	q	inv.	dim.
4	$10/7 \approx 1.43$	$2/7 \approx 0.286$	$\mathcal{L}$	$[x]^7[t]^{-2}$
3	$8/6 \approx 1.33$	$2/6 \approx 0.333$		
2	$6/5 = 1.20$	$2/5 = 0.400$		
1	$4/4 = 1.00$	$2/4 = 0.500$	$\langle A_{\mathrm{2D}}^2 \rangle$	$[x]^4[t]^{-2}$
0	$2/3 \approx 0.67$	$2/3 \approx 0.667$	$\langle A \cdot B \rangle$	$[x]^3[t]^{-2}$
−1	$0/2 = 0.00$	$2/1 = 1.000$		

$$\mathcal{E}_i(t) \sim t^{-p_i} \text{ for } i = \mathrm{K} \text{ or } \mathrm{M}$$

$$\xi \propto t^q,$$

Brandenburg & Kahniashvili 2017

dynamo effect and chiral cascade

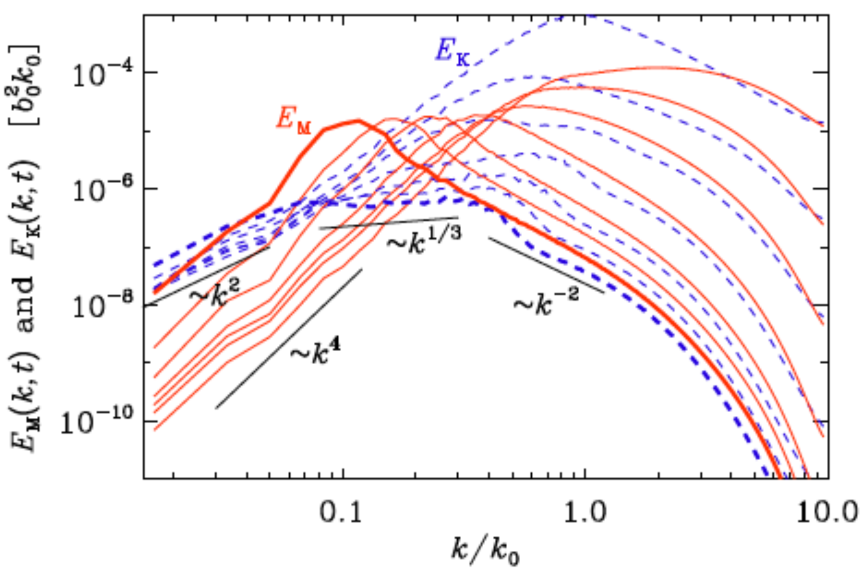

FIG. 2: $E_K(k,t)$ and $E_M(k,t)$ for $t/\tau = 16$, 60, 200, 800, 2000, 6000, and 14,000.

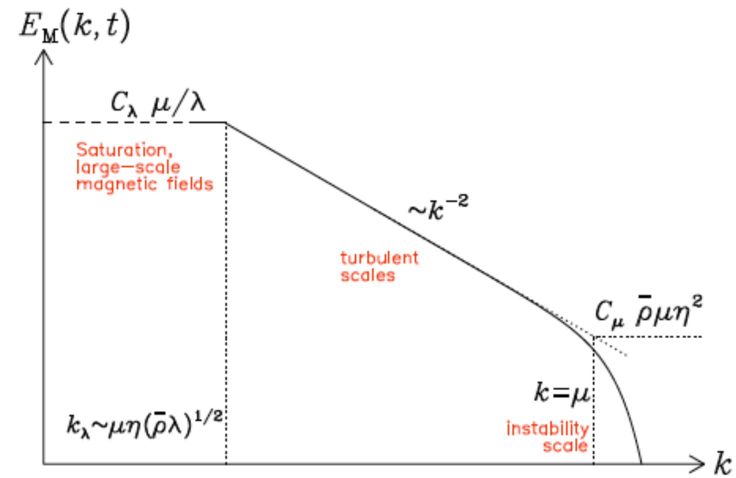

FIG. 1.— Sketch of the magnetic energy spectrum of chiral-magnetically driven turbulence.

Brandenburg, et al. 2017b

$$\mathcal{E}_i(t) \sim t^{-p_i} \text{ for } i = \mathrm{K} \text{ or } \mathrm{M}$$

$$\xi \propto t^q,$$

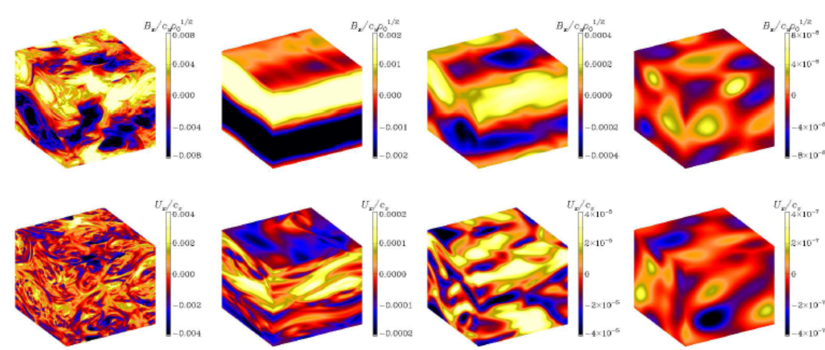

FIG. 3.— B_x and U_x on the periphery of the computational domain for (from left to right) $v_\lambda/v_\mu = 700$, 70, 7, and 0.07 at the last time.

Brandenburg, et al. 2017a

inflationary magnetogensis

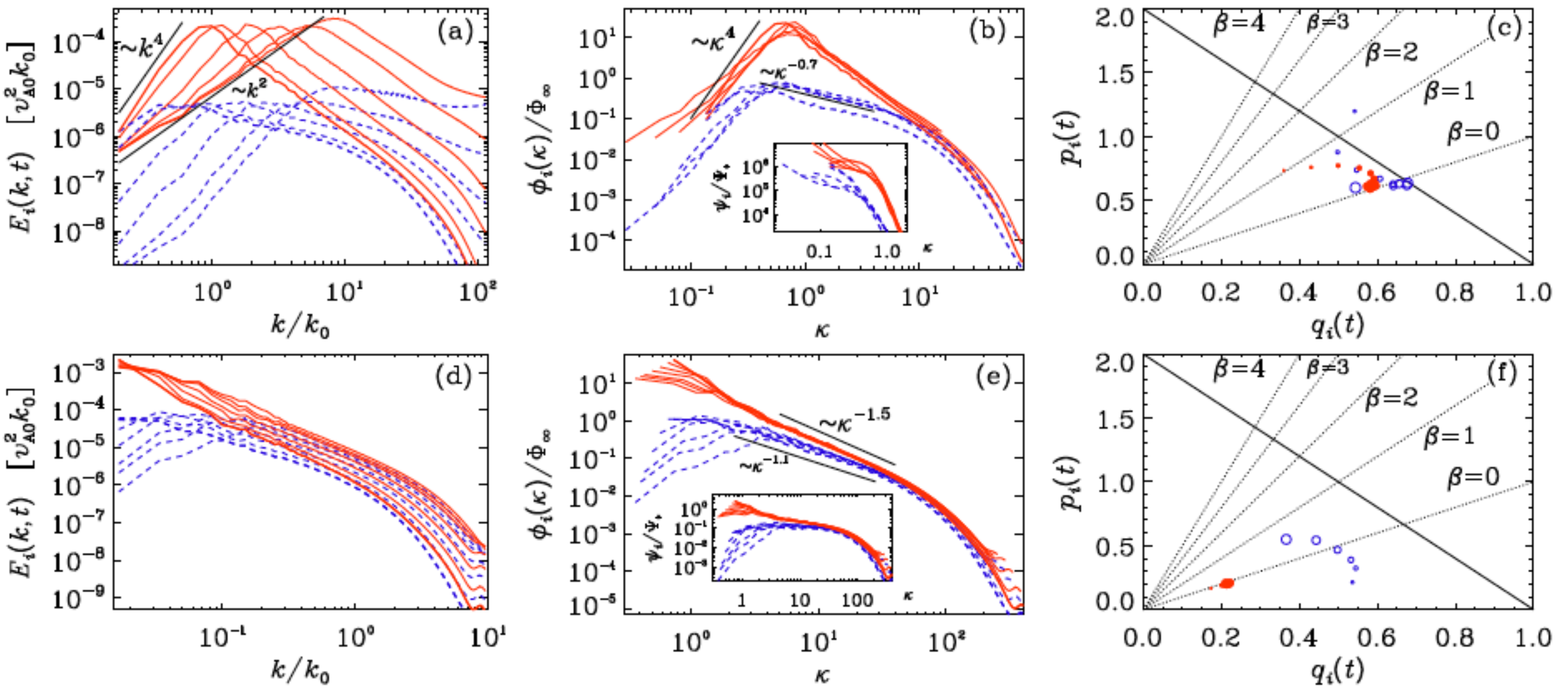

FIG. 3: $E_{\rm M}$ (solid) and $E_{\rm K}$ (dashed) in MHD with fractional helicity and $\alpha = 2$ (a), as well as full helicity and $\alpha = -1$ (d), together with compensated spectra (b,e) and the pq diagrams (c,f).

Brandenburg & Kahniashvili 2017

outcomes fields

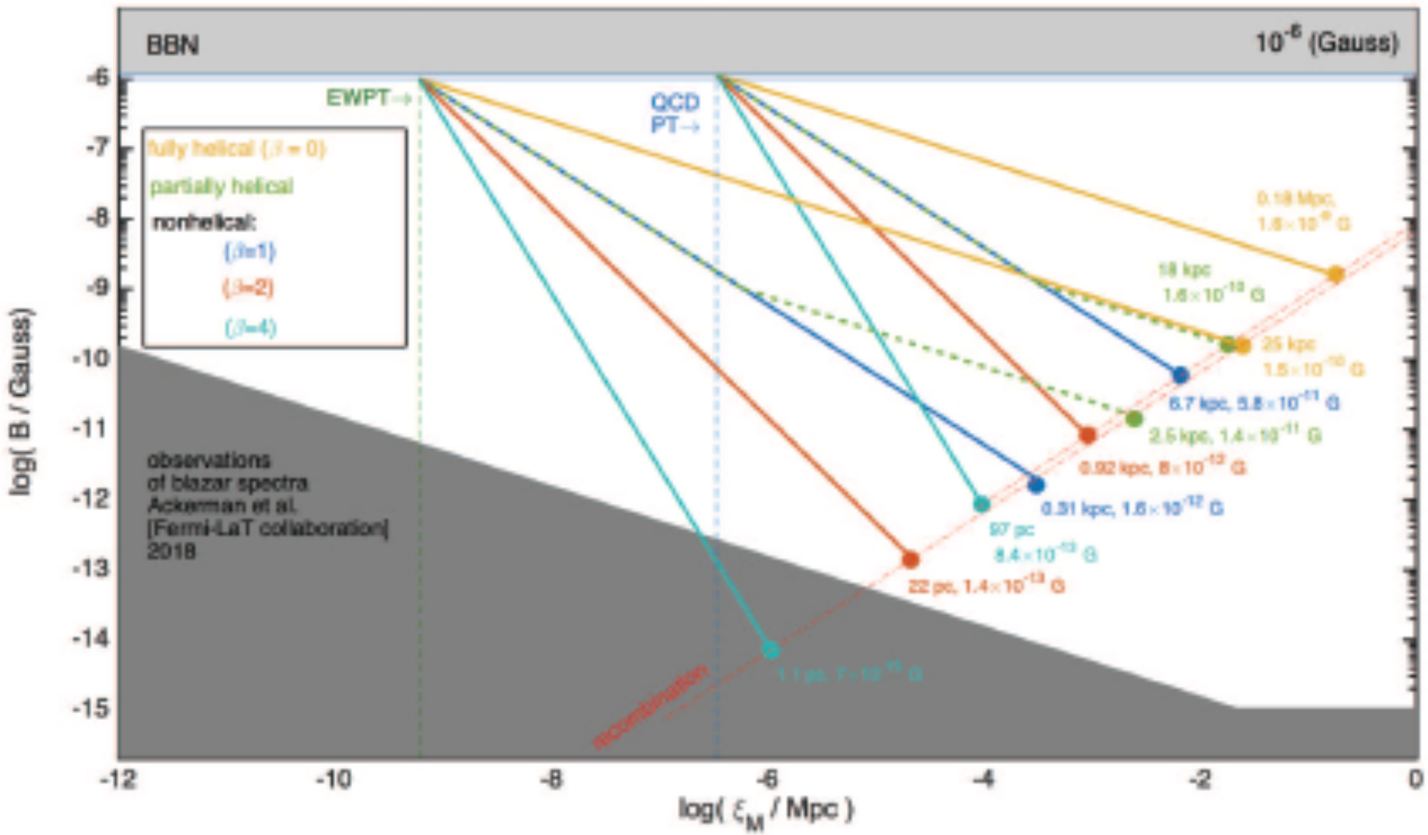

Credit: Emma Clarke

evolution through structure formation

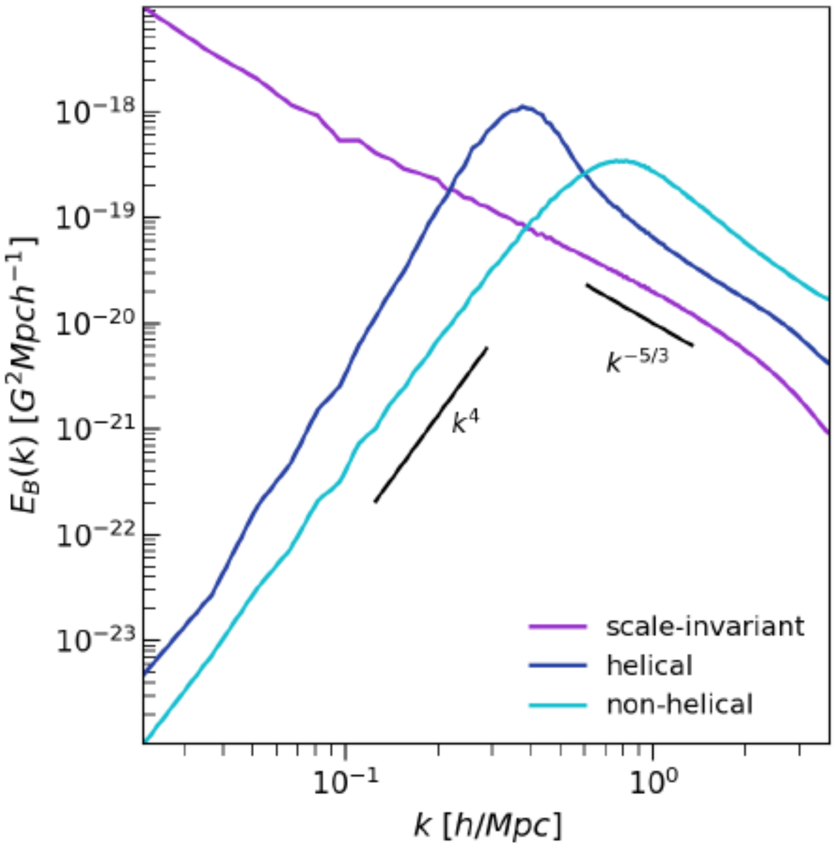

Figure 1. The initial magnetic power spectra for the stochastic setups.

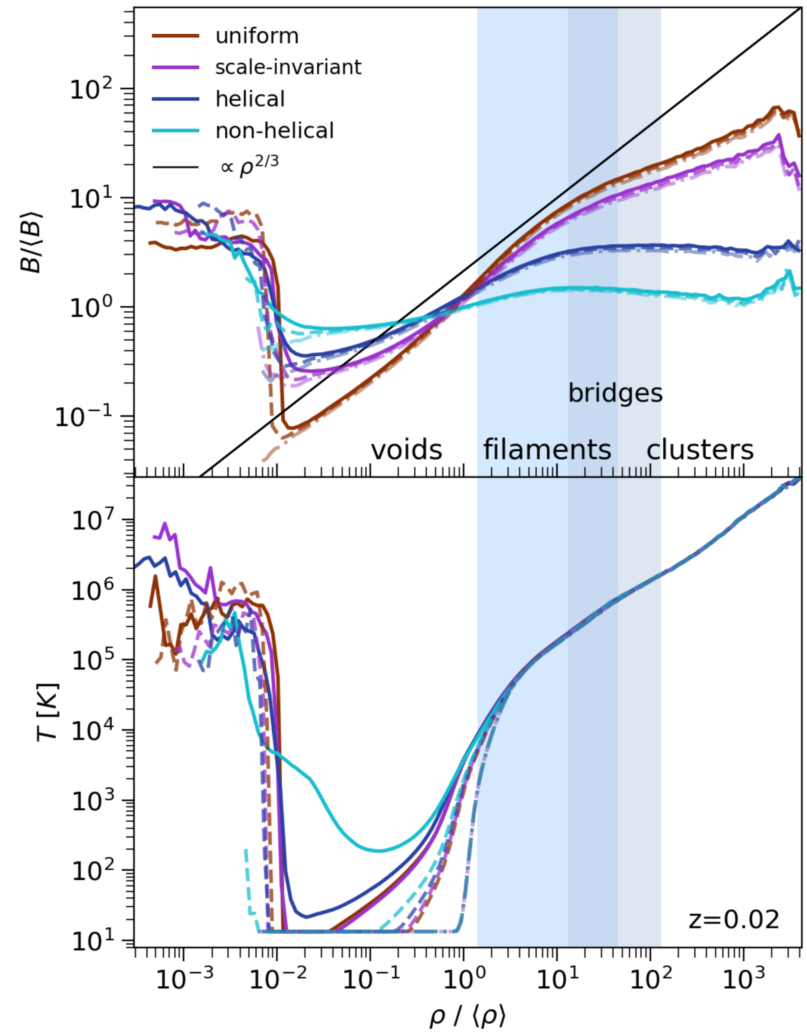

Mtchedlidze et al, 2021

evolution through structure formation

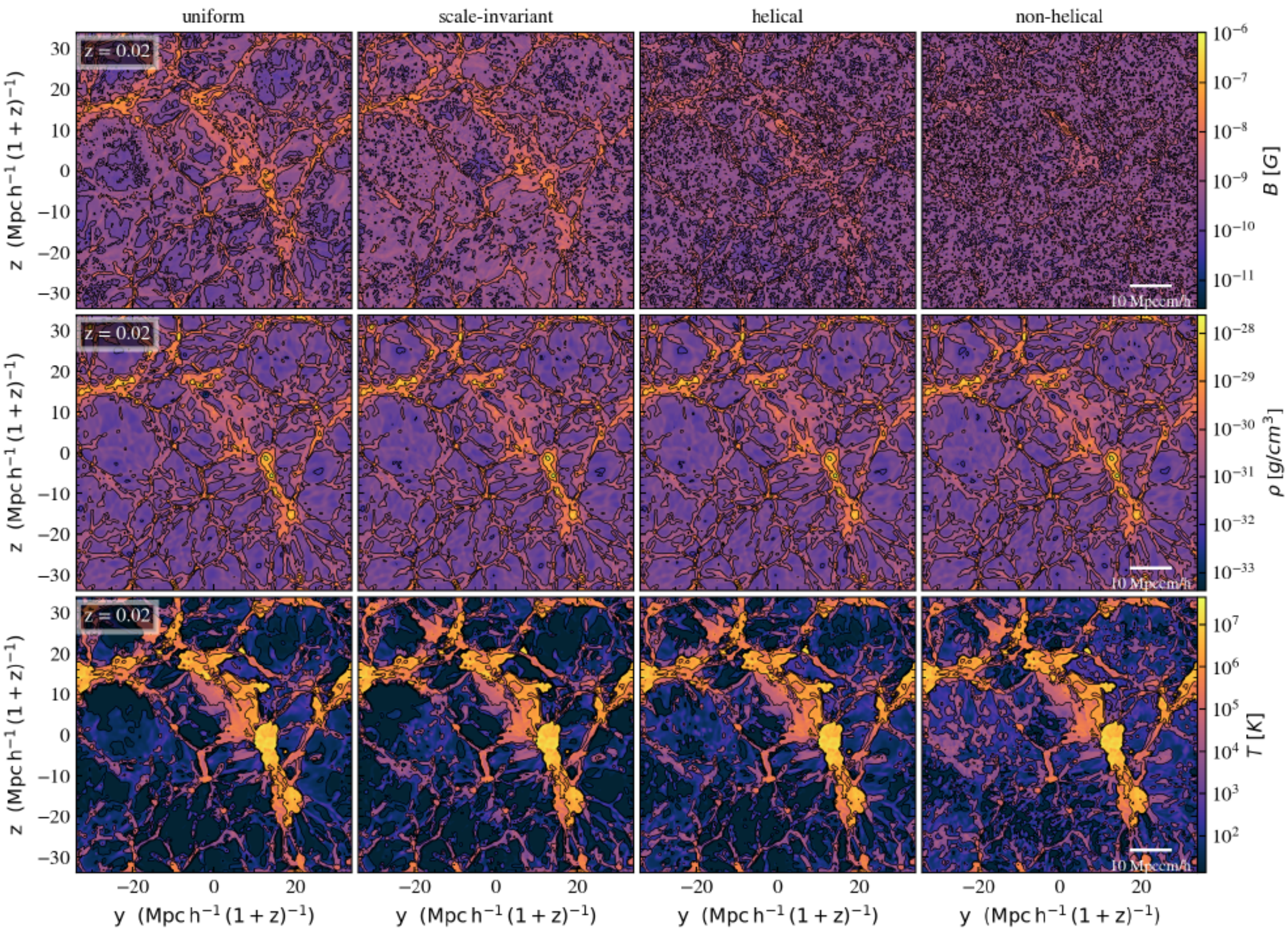

Figure 3. The contoured slices through the center of the simulated box at $z = 0.02$. The top, middle, and bottom panels show the magnetic field, density and temperature slices correspondingly. The overplotted contour lines mark the regions with a certain field strength and the range of the field values are set according to the minimum and maximum of the annotated fields.

Mtchedlidze et al, 2021

evolution through structure formation

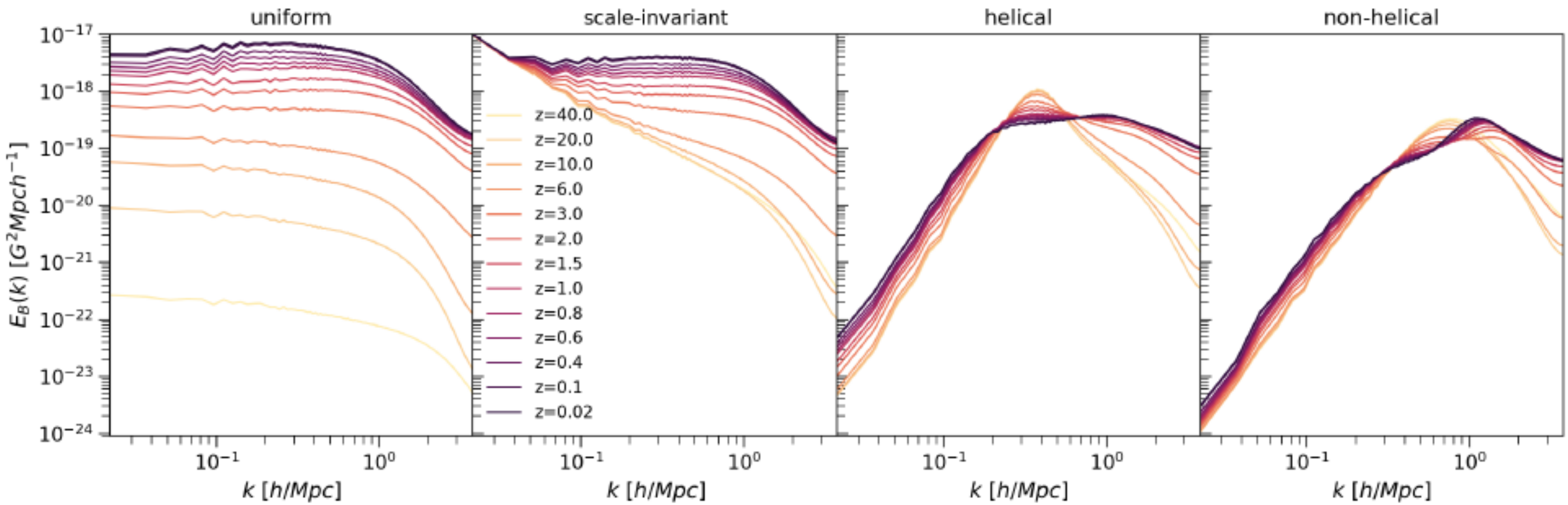

Figure 6. Redshift evolution of magnetic power spectra; from left to right: the uniform, scale-invariant, helical and non-helical seedings.

Mtchedlidze et al, 2021

Primordial Turbulence Signatures

observational signatures include

Density perturbations - scalar mode

- Fast and slow magnetosound waves

Vorticity perturbations - vector mode

- Alfven waves

Gravitational waves - tensor Mode

- No analogy in Newtonian description

$$G_{ik} = 8\pi G T_{ik}$$

Early Universe

- BBN & N_{eff}
- CMB temperature and polarization anisotropies
- Gravitational waves

Late Stages

- Matter power spectrum
- Jeans scale
- LSS clustering

observational signatures

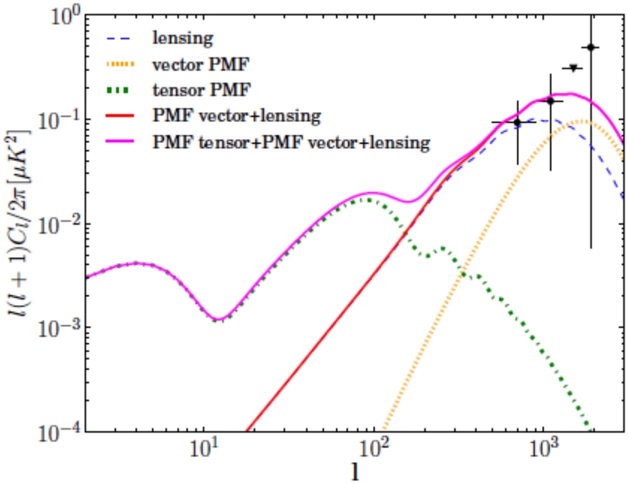

FIG. 4: A representative B-mode polarization power spectrum sourced by a scale-invariant PMF. Shown are the passive tensor mode (green), the compensated vector mode (orange), the gravitational lensing contribution (blue) and the combinations of the lensing and vector B modes (red) and all three components (magenta). The PMF contribution is based on $B_{1\mathrm{Mpc}} = 2.5$ nG, $n = -2.9$, $a_\nu/a_{\mathrm{PMF}} = 10^9$. The data points are from the POLARBEAR first-season B-mode power spectrum. The third point is the 95% upper limit assuming the band power is positive.

POLARBEAR 2015

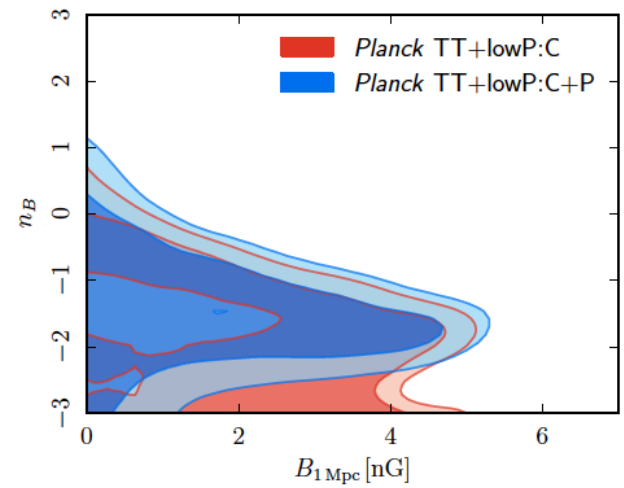

Fig. 8. PMF amplitude versus the spectral index for the baseline *Planck* 2015 case. C+P denotes the case where both compensated and passive modes are considered, whereas C indicates the case with only compensated modes. The two contours represent the 68 % and 95 % confidence levels.

Planck 2015 Results

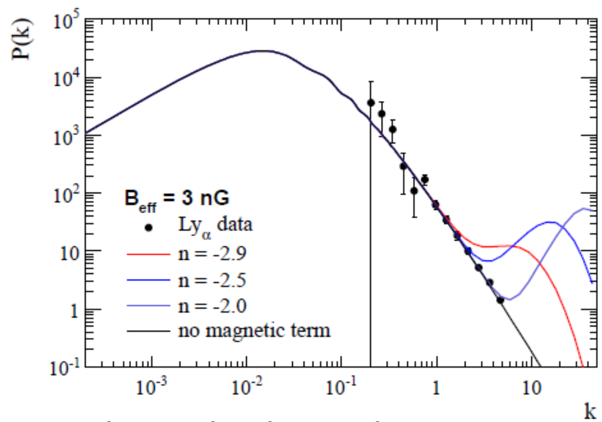

Data:
Croft et al. 2002

Kahniashvili et al. 2013

gravitational waves primordial turbulence?

$$\nabla^2 \delta\rho(\boldsymbol{x},t) - \frac{1}{c_s^2}\frac{\partial^2}{\partial t^2}\delta\rho(\boldsymbol{x},t) = -\frac{\partial^2}{\partial x^i \partial x^j}T(\boldsymbol{x},t), \qquad c_s^2 = \frac{\partial p}{\partial \rho}$$

$$\nabla^2 h_{ij}(\boldsymbol{x},t) - \frac{\partial^2}{\partial t^2}h_{ij}(\boldsymbol{x},t) = -16\pi G\, S_{ij}(\boldsymbol{x},t) \qquad c = 1$$

Aero-acoustic approximation:

✓ sound waves generation by turbulence

✓ gravitational waves generation

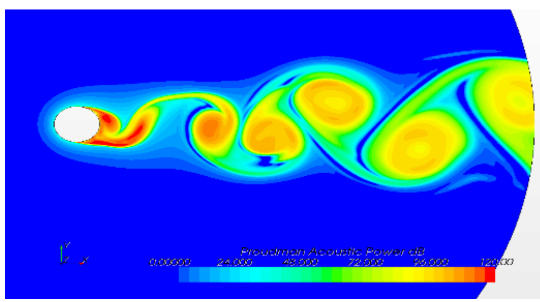

Lighthill, 1952; Proudman 1952

Kosowsky, Mack, Kahniashvili, 2002
Dolgov, Grasso, Nicolis, 2002

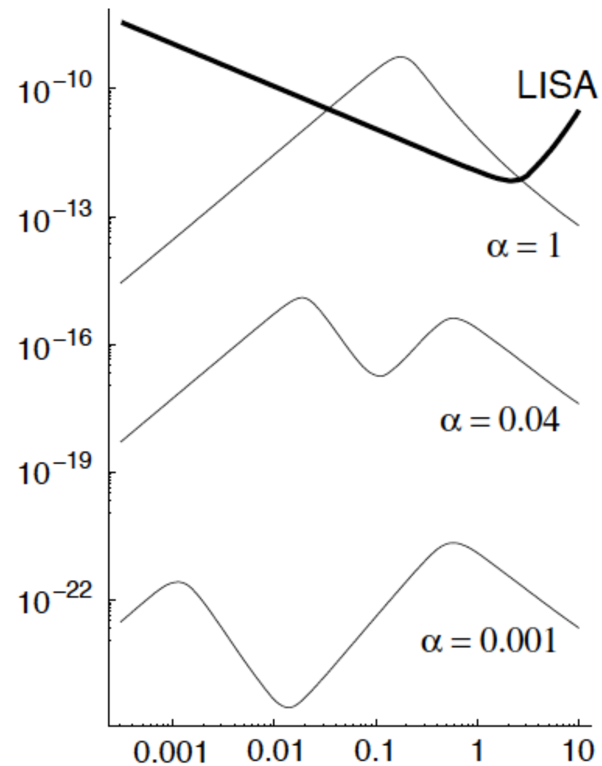

Nicolis 2004

NANOGrav 12.5 years observations:

NANOGrav 12.5-year sensitivity range of 1–100 nHz

$$h_c(f) = A_{\rm CP}\left(\frac{f}{f_{\rm yr}}\right)^{\alpha_{\rm CP}},$$

$$\Omega_{\rm GW}(f) = \frac{2\pi^2}{3H_0^2} f^2 h_c^2(f) = \Omega_{\rm GW}^{\rm yr}\left(\frac{f}{f_{\rm yr}}\right)^{5-\gamma_{\rm CP}}$$

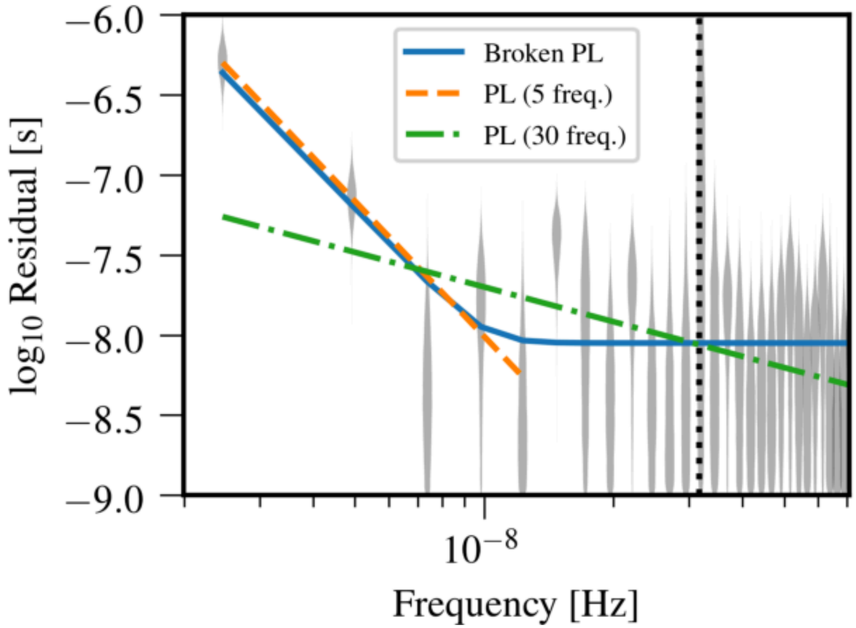

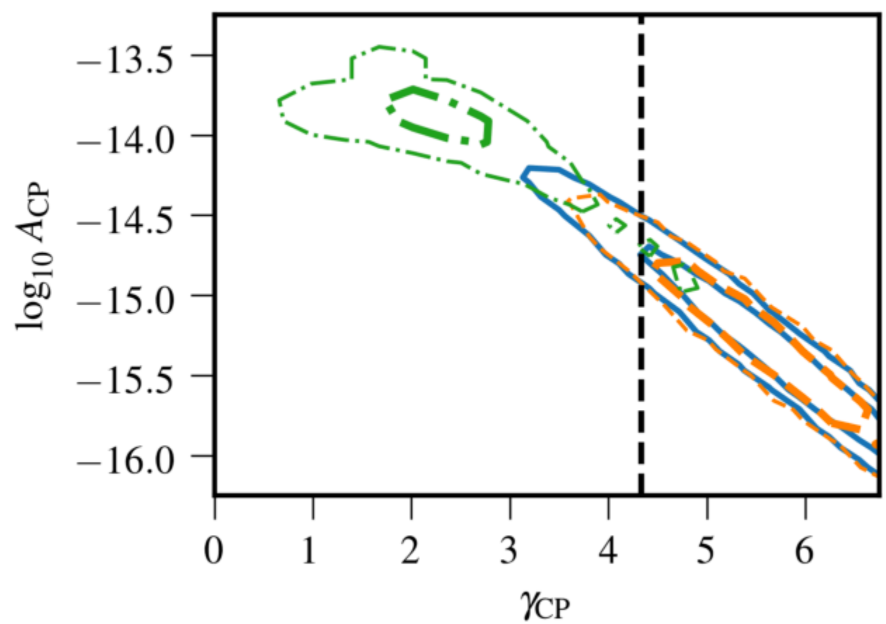

$$\Omega_{\rm GW}(t,f) = \frac{1}{\mathcal{E}_{\rm crit}(t)}\frac{{\rm d}\mathcal{E}_{\rm GW}}{{\rm d}\ln f}$$

Arzoumanian et al (2021)

Possible Sources:

Astrophysical:

- ✓ Super massive black hole binary (SMBHB) (Phinney 2001): γ=13/3

Cosmological:

- ✓ Bubbles collisions (Kosowsky et. Al. 1993)
- ✓ Inflation (Vagnozzi 2021)
- ✓ Cosmic strings (Blanco-Pillado et al. 2021)
- ✓ Seed magnetic fields (Neronov et. al. 2021)
- ✓ Hydrodynamic and MHD Turbulence (Brandenburg et al. 2021)

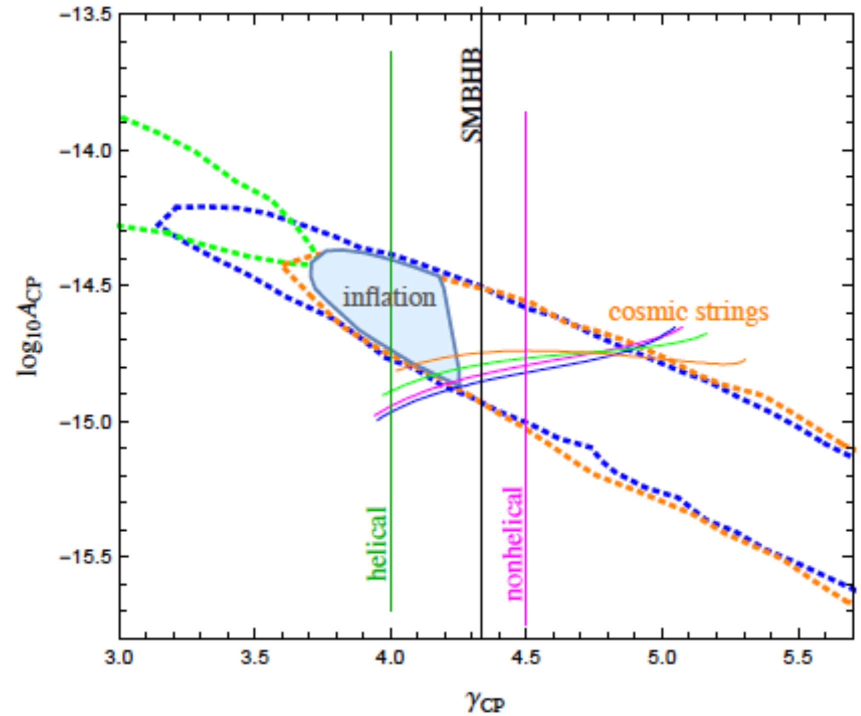

Credit: Emma Clarke

QCD energy scale

$$\frac{a_0}{a_\star} = 10^{12}\left(\frac{g_{S,\star}}{15}\right)^{\frac{1}{3}}\left(\frac{T_\star}{150\text{ MeV}}\right)$$

$$H_\star^2 = \frac{8\pi G}{2}\mathcal{E}_{\text{rad},\star} \qquad \mathcal{E}_{\text{rad},\star} = \frac{\pi^2 g_\star}{30}T_\star^4 \qquad (c = k_B = \hbar = 1)$$

$$f_H \simeq (1.8\times 10^{-8}\text{Hz})10^{12}\left(\frac{g_\star}{15}\right)^{\frac{1}{3}}\left(\frac{T_\star}{150\text{ MeV}}\right)$$

numerical simulations

- ✓ To account properly non-linear processes (MHD)
- ✓ Not be limited by the short duration of the phase transitions
- ✓ Two stages turbulence decay
    - Forced turbulence
    - Free decay
- ✓ The source is present till recombination (after the field is frozen in)
- ✓ Results – strongly initial conditions dependent

$$\left(\frac{\partial^2}{\partial t^2} - c^2\nabla^2\right) h_{ij}^{\mathrm{TT}} = \frac{16\pi G}{a^3 c^2} T_{ij}^{\mathrm{TT}},$$

$$h_{ij}^{\mathrm{TT}} = a h_{ij}^{\mathrm{TT,phys}} \qquad \mathrm{d}t_{\mathrm{phys}} = a\mathrm{d}t$$

Brandenburg et al (2021)

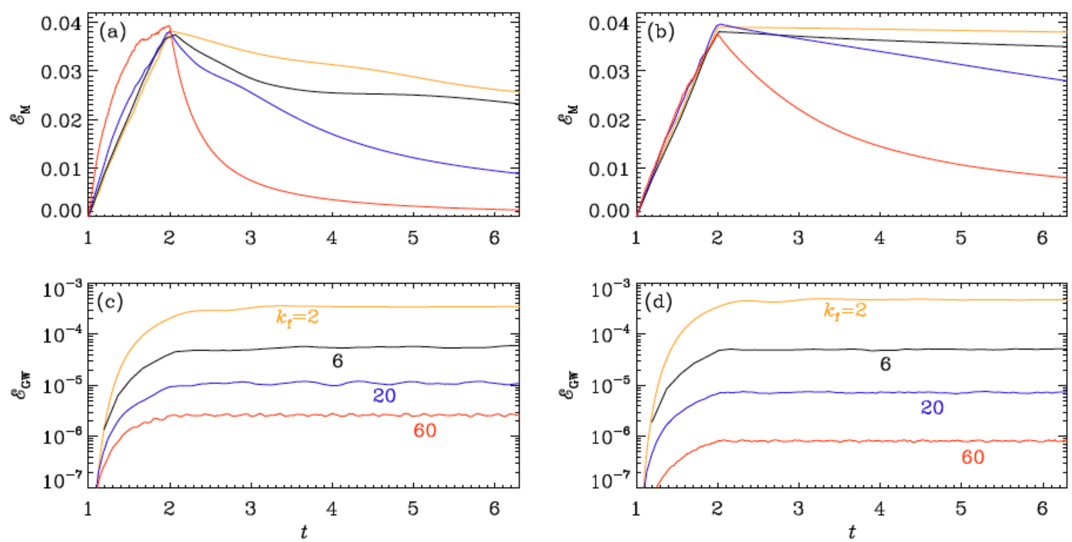

$$\mathcal{E}_{\mathrm{M}}(t) = \mathcal{E}_{\mathrm{M}}^{\max}\left(1 + \Delta t/\tau\right)^{-p}$$

$$\mathcal{E}_{\mathrm{GW}}^{\mathrm{sat}} = \left(q\mathcal{E}_{\mathrm{M}}^{\max}/k_{\mathrm{f}}\right)^2$$

Evolution of $E_M(t)$ and $E_{GW}(t)$ for nonhelical (left) and helical (right) cases. Orange, black, blue, and red are for k_f = 2, 6, 20, and 60, respectively.

Results

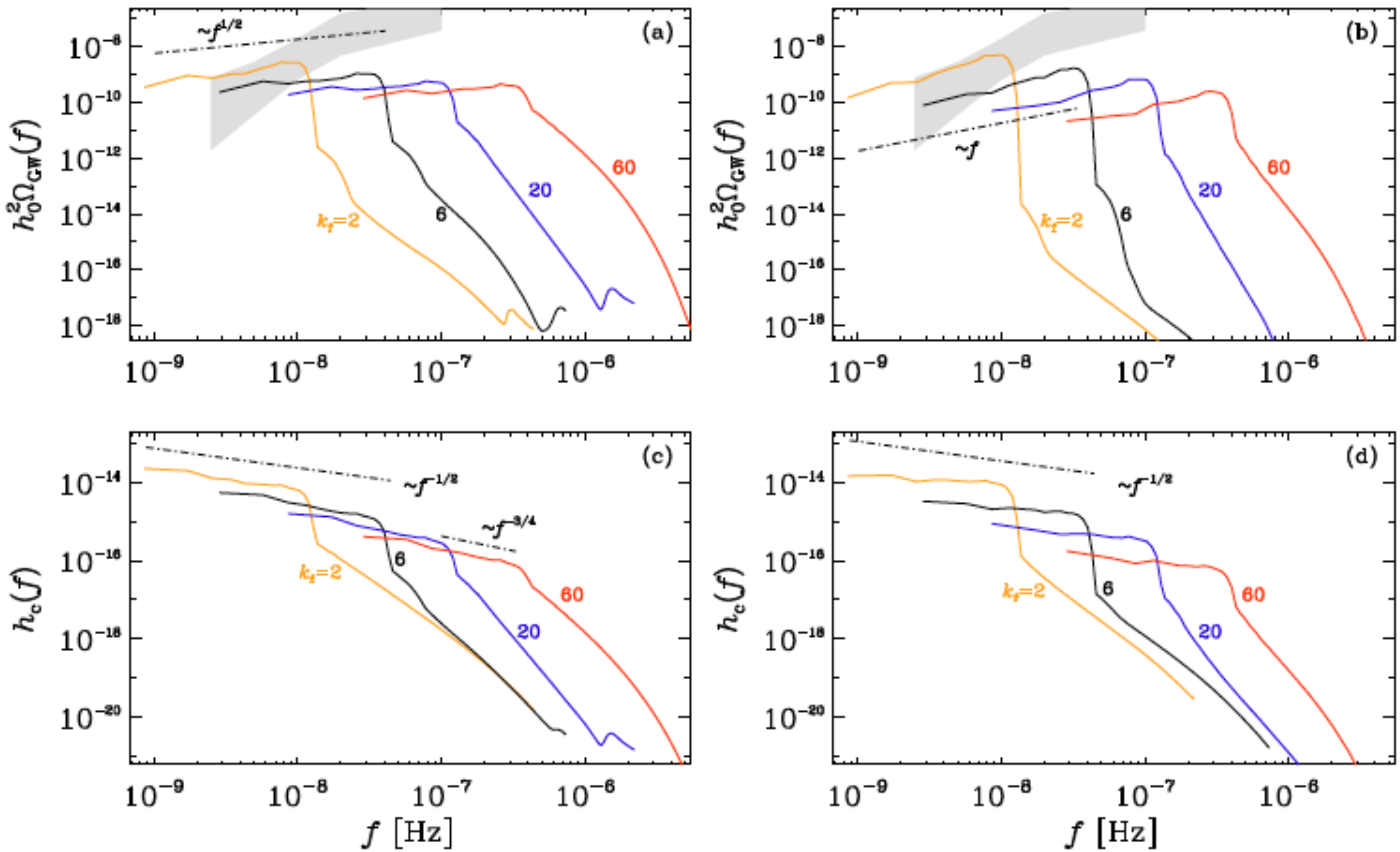

FIG. 5: $h_0^2\Omega_{\rm GW}(f)$ and $h_c(f)$ at the present time for all four runs presented in Table I, for the nonhelical (left) and helical (right) runs. The 2σ confidence contour for the 30-frequency power law of the NANOGrav 12.5-year data set is shown in gray.

Brandenburg et al (2021) [arXiv:2102.12428]

Next steps

Determine the mechanisms insuring the presence of viable turbulent sources and correspondingly correct initial conditions:

- ❖ Primordial magnetogenesis
- ❖ Bubble collisions/nucleation – more realistic models
- ❖ Sound waves as a source for turbulence
- ❖ Axions driven turbulence and axion like particles driven inflationary new physics
- ❖ Cihiral sources and gravitational waves polarization
- ❖ Low temperature re and pre-heating

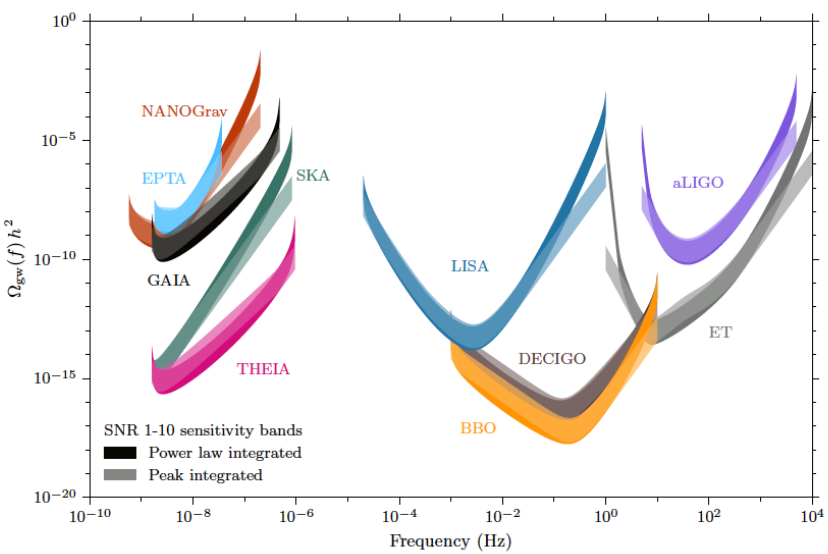

Cross-correlating data between different observations:

- ❖ PTAs
- ❖ Astrometric missions: Gaia, Theia

$$\Omega_{\rm gw}(f)\,h^2 = \frac{2\pi^2}{3H_0^2} f^2 h_{\rm gw}^2(f) h^2$$

Garcia-Bellido et al. 2021
arXiv: 2104.04778

conclusion

- The high conductivity of primordial plasma insures possibility of hydro and magneto-hydrodynamics turbulence development in the early universe
- Turbulence experiences decay through the expansion of the universe
- Primordial MHD turbulence is a plausible explanation of the observed magnetic fields in galaxies, clusters, and voids (if confirmed)
- Primordial turbulence signatures include:
  - gravitational waves
  - cosmic microwave background fluctuations
  - effects of the matter power spectrum (large scale structure)

Thank You!

Questions?